Sociedade Brasileira de Eletroquímica e Eletroanalítica
SBEE

Eclética Química Journal

Volume 44 • special issue • year 2019

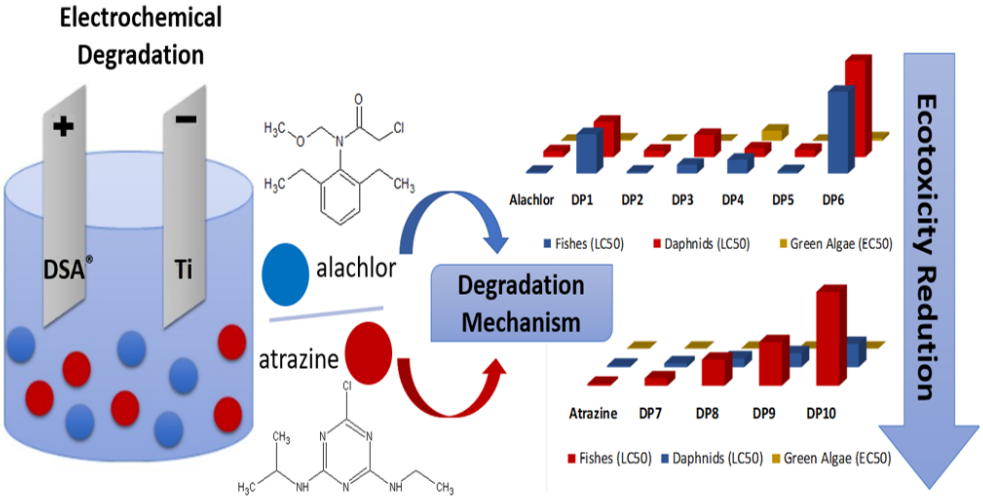

Electrochemical degradation of aqueous alachlor and atrazine: products identification, lipophilicity, and ecotoxicity

Electrodeposition

Electrodeposition study of the Cu-Zn-Mo system in citrate/sulfate medium

Electrodialysis

Application of ultrafiltration and electrodialysis techniques in lactic acid removal from whey solutions

Ethanol

Membraneless ethanol,O_2 enzymatic biofuel cell based on laccase and ADH/NAD^+ bioelectrodes

unesp
UNIVERSIDADE ESTADUAL PAULISTA
"JÚLIO DE MESQUITA FILHO"

Instituto de Química
UNESP
Araraquara
ISSN 1678-4618

UNIVERSIDADE ESTADUAL PAULISTA

Reitor

Sandro Roberto Valentini

Vice-reitor

Sergio Roberto Nobre

Pró-reitor de Planejamento Estratégico e Gestão

Leonardo Theodoro Büll

Pró-reitora de Graduação

Gladis Massini-Cagliari

Pró-reitora de Pós-Graduação

Telma Teresinha Berchielli

Pró-reitora de Extensão Universitária

Cleopatra da Silva Planeta

Pró-reitor de Pesquisa

Carlos Frederico de Oliveira Graeff

INSTITUTO DE QUÍMICA

Diretor

Eduardo Maffud Cilli

Vice-Diretora

Dulce Helena Siqueira Silva

Eclética Química Journal

Editorial board
iq.unesp.br/ecletica

| Vol. 44 | special issue | 2019 |

Editorial Team

Eclética Química Journal

Editorial
iq.unesp.br/ecletica

| Vol. 44 | special issue | 2019 |

Editorial

First Meeting of Electrochemistry and Electroanalytical Brazilian Society (SBEE)

The Electrochemistry and Electroanalytical Brazilian Society has organized its first event as a national forum for scientific and academic discussions. The meeting theme was "*Environmental Challenges for a Sustainable Progress in the 21st Century*" focused on the energy and environment subject aiming at discussing the Electrochemistry and Electroanalytical contributions in these areas. SBEE's goal is to hold meetings every two years on specific topics in order to promote greater interaction between members of society and researchers around subjects that are relevant to the progress of science and society in general. The SBEE board members and researchers of the University of São Paulo (USP) at Ribeirão Preto and of the Federal University of ABC (UFABC) organized the event that occurred on November 8th and 9th, 2018 in Ribeirão Preto (SP) at the campus of the University of São Paulo. There was a significant number of abstracts submitted, suggesting the need of periodic continuity of this topical meeting. In addition to the participation of renowned Brazilian researchers, guest speakers from France also attended this event. Indeed Prof. Mehmet A. Otturan, from University of Paris-EST, France presented "*The use of new photoactive materials for treatment of organic pollutants*"; continuing on this theme Prof. Romeu Rocha Filho (UFSCar/SP) presented the main actions to be taken in the construction of electrochemical reactors, presenting the plenary lecture "*Hurdles to cross to make electrochemical oxidation a sustainable technology*". Advances in the characterization of more active nanomaterials were presented by Prof. Teko Napporn from University of Poitiers, France "*Gold Nanospheres in electrocatalysis: surface interaction with glucose*" and Dr. Fabio Henrique Barros Lima (IQSC/USP) "*Advances in the electrocatalysis of oxygen and carbon dioxide reduction*".

Besides these, four plenary lectures from invited speakers the meeting had 148 inscriptions, 105 papers presented, being 25 oral presentations. Additionally, the meeting offered the opportunity for researchers publishing their peer-reviewed results in this special issue of Eclética Química Journal. We thank the authors and the reviewers for the suggestions and comments.

Profa. Dra. Adalgisa Rodrigues de Andrade (Guest Editor)
Prof. Dr. Paulo Olivi (Guest Editor)

Eclética Química Journal

Editor's note
iq.unesp.br/ecletica

| Vol. 44 | special issue | 2019 |

Editor's note

The articles published in this special issue went through all the standard procedures used by the Eclética Química Journal and fulfilled all the qualitative requirements of selection, peer review and editing.

The readers can see the papers cover the Electrochemistry and Electroanalytical areas, in line with the editorial profile of EQJ, with the following subjects: electrochemical degradation of aqueous alachlor and atrazine; electrodeposition of Cu-Zn-Mo system; ultrafiltration and electrodialysis on lactic acid removal from whey and membraneless ethanol,O_2 enzymatic biofuel cell.

Prof. Dr. Assis Vicente Benedetti
Editor-in-Chief

Eclética Química Journal

Author guidelines
iq.unesp.br/ecletica

| Vol. 44 | special issue | 2019 |

Instructions for Authors

Preparation of manuscripts

• **Only manuscripts in English will be accepted.** British or American usage is acceptable, but they should not be mixed.

• **The corresponding author should submit the manuscript online at**
http://revista.iq.unesp.br/ojs/index.php/ecletica/author

• **Manuscripts must be sent in editable files as** *.doc, *.docx or *.odt. The text must be typed using font style Times New Roman and size 11. Space between lines should be 1.5 mm and paper size A4.

• **The manuscript should be organized in sections as follows:** Introduction, Experimental, Results and Discussion, Conclusions, and References. Sections titles must be written in bold and sequentially numbered; only the first letter should be in uppercase letter. Subsections should be written in normal and italic lowercase letters. For example: **1. Introduction**; *1.1 History;* **2. Experimental**; *2.1 Surface characterization; 2.1.1 Morphological analysis.*

• **The cover letter should include**: the authors' full names, e-mail addresses, ORCID code and affiliations, and remarks about the novelty and relevance of the work. The cover letter should also contain a declaration of the corresponding author, on behalf of the other authors, that the article being submitted is original and its content has not been published previously and is not under consideration for publication elsewhere, that no conflict of interest exists and if accepted, the article will not be published elsewhere in the same form, in any language, without the written consent of the publisher. Finally, the cover letter should also contain the suggestion of 3 (three) suitable reviewers (please, provide full name, affiliation, and e-mail).

• **The first page of the manuscript** should contain the title, abstract and keywords. **Please, do not give authors names and affiliation, and acknowledgements since a double-blind review system is used. Acknowledgements should be added to the proof only.**

• **All contributions should include** an Abstract (200 words maximum), three to five Keywords and a Graphical Abstract (8 cm wide × 4 cm high) with an explicative text (2 lines maximum).

• **Citations should be sequentially numbered** and presented in square brackets throughout the text, and references should be compiled in square brackets at the end of the manuscript as follows:

***Journal*:**

[1] Adorno, A. T. V., Benedetti, A. V., Silva, R. A. G. da, Blanco, M., Influence of the Al content on the phase transformations in Cu-Al-Ag Alloys, Eclet. Quim. 28 (1) (2003) 33-38. https://doi.org/10.1590/S0100-46702003000100004.

***Book*:**

[2] Wendlant, W. W., Thermal Analysis, Wiley-Interscience, New York, 3rd ed., 1986, ch1.

***Chapter in a book*:**

[3] Ferreira, A. A. P., Uliana, C. V., Souza Castilho, M. de, Canaverolo Pesquero, N., Foguel, N. V., Pilon dos Santos, G., Fugivara, C. S., Benedetti, A. V., Yamanaka, H., Amperometric Biosensor for Diagnosis of Disease, In: State of the Art in Biosensors - Environmental and Medical Applications, Rinken, T., ed., InTech: Rijeka, Croatia, 2013, Ch. 12.

***Material in process of publication*:**

[4] Valente Jr., M. A. G., Teixeira, D. A., Lima Azevedo, D., Feliciano, G. T., Benedetti, A. V., Fugivara, C. S., Caprylate Salts Based on Amines as Volatile Corrosion Inhibitors for Metallic Zinc: Theoretical and Experimental Studies, Frontiers in Chemistry. https://doi.org/10.3389/fchem.2017.00032.

• Figures, Schemes, and Tables should be numbered sequentially and presented at the end of the manuscript.

• Nomenclature, abbreviations, and symbols should follow IUPAC recommendations.

• Figures, schemes, and photographs already published by the same or different authors in other publications may be reproduced in manuscripts of **Eclet. Quim. J.** only with permission from the editor house that holds the copyright.

• Graphical Abstract (GA) should be a high-resolution figure (900 dpi) summarizing the manuscript in an interesting way to catch the attention of the readers and accompanied by a short explicative text (two lines maximum). GA must be submitted as *.jpg, *.jpeg or *.tif.

• **Communications** should cover relevant scientific results and are limited to 1,500 words or three pages of the Journal, not including the title, authors' names, figures, tables and references. However, Communications suggesting fragmentation of complete contributions are strongly discouraged by Editors.

• **Review articles** should be original and present state-of-the-art overviews in a coherent and concise form covering the most relevant aspects of the topic that is being revised and indicate the likely future directions of the field. Therefore, before beginning the preparation of a Review manuscript, send a letter (one page maximum) to the Editor with the subject of interest and the main topics that would be covered in the Review manuscript. The Editor will communicate his decision in two weeks. Receiving this type of manuscript does not imply acceptance to be published in **Eclet. Quím. J.** It will be peer-reviewed.

• **Short reviews** should present an overview of the state-of-the-art in a specific topic within the scope of the Journal and limited to 5,000 words. Consider a table or image as corresponding to 100 words. Before beginning the preparation of a Short Review manuscript, send a letter (one page maximum) to the Editor with the subject of interest and the main topics that would be covered in the Short Review manuscript.

• **Technical Notes**: descriptions of methods, techniques, equipment or accessories developed in the authors' laboratory, as long as they present chemical content of interest. They should follow the usual form of presentation, according to the peculiarities of each work. They should have a maximum of 15 pages, including figures, tables, diagrams, etc.

• **Articles in Education in Chemistry and chemistry-correlated areas**: research manuscript related to undergraduate teaching in Chemistry and innovative experiences in undergraduate and graduate education. They should have a maximum of 15 pages, including figures, tables, diagrams, and other elements.

Special issues with complete articles dedicated to Symposia and Congresses can be published by **Eclet. Quim. J.** under the condition that a previous agreement with Editors is established. All the guides of the journal must be followed by the authors.

Eclet. Quim. J. Ethical Guides and Publication Copyright:

Before beginning the submission process, please be sure that all ethical aspects mentioned below were followed. Violation of these ethical aspects may prevent authors from submitting and/or publishing articles in **Eclet. Quim. J.**

- The corresponding author is responsible for listing as coauthors only researchers who have really taken part in the work, for informing them about the entire manuscript content and for obtaining their permission to submit and publish it.

- Authors are responsible for carefully searching for all the scientific work relevant to their reasoning irrespective of whether they agree or not with the presented information.

- Authors are responsible for correctly citing and crediting all data used from works of researchers other than the ones who are authors of the manuscript that is being submitted to **Eclet. Quim. J.**

- Citations of Master's Degree Dissertations and PhD Theses are not accepted; instead, the publications resulting from them must be cited.

- Explicit permission of a nonauthor who has collaborated with personal communication or discussion to the manuscript being submitted to **Eclet. Quím. J.** must be obtained before being cited.

- Simultaneous submission of the same manuscript to more than one journal is considered an ethical deviation and is conflicted to the declaration has been done below by the authors.

- Plagiarism, self-plagiarism, and the suggestion of novelty when the material was already published are unaccepted by **Eclet. Quim. J.**

- The word-for-word reproduction of data or sentences as long as placed between quotation marks and correctly cited is not considered ethical deviation when indispensable for the discussion of a specific set of data or a hypothesis.

- Before reviewing a manuscript, the *Turnitin* antiplagiarism software will be used to detect any ethical deviation.

- The corresponding author transfers the copyright of the submitted manuscript and all its versions to **Eclet. Quim. J.**, after having the consent of all authors, which ceases if the manuscript is rejected or withdrawn during the review process.

- Before submitting manuscripts involving human beings, materials from human or animals, the authors need to confirm that the procedures established, respectively, by the institutional committee on human experimentation and Helsinki's declaration, and the recommendations of the animal care institutional committee were followed. Editors may request complementary information on ethical aspects.

- When a published manuscript in EQJ is also published in other Journal, it will be immediately withdrawn from EQJ and the authors informed of the Editor decision.

• Manuscript Submissions

For the first evaluation: the manuscripts should be submitted in three files: the cover letter as mentioned above, the graphical abstract and the entire manuscript.

The entire manuscript should be submitted as *.doc, *.docx or *.odt files.

The Graphical Abstract (GA) 900 dpi resolution is mandatory for this Journal and should be submitted as *.jpg, *.jpeg or *.tif files as supplementary file.

The cover letter should contain the title of the manuscript, the authors' names and affiliations, and the relevant aspects of the manuscript (no more than 5 lines), and the suggestion of 3 (three) names of experts in the subject: complete name, affiliation, and e-mail).

When appropriate, important data to complement and a better comprehension of the article can be submitted as Supplementary File, which will be published online and will be made available as links in the original article. This might include additional figures, tables, text, equations, videos or other materials that are necessary to fully document the research contained in the paper or to facilitate the readers' ability to understand the work. Supplementary Materials should be presented in appropriate .docx file for text, tables, figures and graphics. The full title of the paper, authors' names and affiliations, and corresponding author should be included in the header. All supplementary figures, tables and videos should be referred in the manuscript body as "Table S1, S2…", "Fig. S1, S2…" and "Video S1, S2 …".

• Reviewing

The time elapsed between the submission and the first response of the reviewers is around 3 months. The average time elapsed between submission and publication is seven months.

• **Resubmission** (manuscripts "rejected in the present form" or subjected to "revision"): **A LETTER WITH THE RESPONSES TO THE COMMENTS/CRITICISM AND SUGGESTIONS OF REVIEWERS/EDITORS SHOULD ACCOMPANY THE REVISED MANUSCRIPT. ALL MODIFICATIONS MADE TO THE ORIGINAL MANUSCRIPT MUST BE HIGHLIGHTED.**

• Editor's requirements

Authors who have a manuscript accepted in **Eclética Química Journal** may be invited to act as reviewers.

Only the authors are responsible for the correctness of all information, data and content of the manuscript submitted to **Eclética Química Journal**. Thus, the Editors and the Editorial Board cannot accept responsibility for the correctness of the material published in **Eclética Química Journal**.

• Proofs

After accepting the manuscript, **Eclet. Quim. J.** technical assistants will contact you regarding your manuscript page proofs to correct printing errors only, i.e., other corrections or content improvement are not permitted. The proofs shall be returned in 3 working days (72 h) via e-mail.

• Authors Declaration

The corresponding author declares, on behalf of the other authors, that the article being submitted is original and has been written by the stated authors who are all aware of its content and approve its submission. Declaration should also state that the article has not been published previously and is not under consideration for publication elsewhere, that no conflict of interest exists and if accepted, the article will not be published elsewhere in the same form, in any language, without the written consent of the publisher.

• Appeal

Authors may only appeal once about the decision regarding a manuscript. To appeal against the Editorial decision on your manuscript, the corresponding author can send a rebuttal letter to the editor, including a detailed response to any comments made by the reviewers/editor. The editor will consider the rebuttal letter, and if dimmed appropriate, the manuscript will be sent to a new reviewer. The Editor decision is final.

• Contact

Gustavo Marcelino de Souza (ecletica@journal.iq.unesp.br)

Submission Preparation Checklist

As part of the submission process, authors are required to check off their submission's compliance with all of the following items, and submissions may be returned to authors that do not adhere to these guidelines.

In **Step 1**, select the appropriate section for this submission.

Be sure that Authors' names, affiliations and aknowledgements were removed from the manuscript. The manuscript must be in *.doc, *.docx or *.odt format before uploading in **Step 2**.

In **Step 3**, add the full name of each author including the ORCID IDs in its full URL ONLY WITH HTTP, NOT HTTPS (e.g. http://orcid.org/0000-0002-1825-0097).

Add the authors in the same order as they appear in the manuscript in **step 3**.

Be sure to have the COVER LETTER and GRAPHICAL ABSTRACT (according to the Author Guidelines) to upload them in **Step 4**.

Check if you've followed all the previous steps before continuing the submission of your manuscript.

Copyright Notice

The corresponding author transfers the copyright of the submitted manuscript and all its versions to **Eclet. Quim. J.**, after having the consent of all authors, which ceases if the manuscript is rejected or withdrawn during the review process.

Self-archive to institutional, thematic repositories or personal web page is permitted just after publication.

Eclética Química Journal

| Vol. 44 | special issue | 2019 |

SUMMARY

Eclética Química Journal

Original article
iq.unesp.br/ecletica

| Vol. 44 | special issue | 2019 |

Electrochemical degradation of aqueous alachlor and atrazine: products identification, lipophilicity, and ecotoxicity

Rafaely Ximenes de Sousa Furtado+, Eduardo Bessa Azevedo, Artur de Jesus Motheo

University of São Paulo (USP), São Carlos Institute of Chemistry, 400 Trabalhador São Carlense Ave, São Carlos, São Paulo, Brazil

+Corresponding author: Rafaely Ximenes de Sousa Furtado, phone: +55 16 3373 9932, email address: rafaelyximenes@hotmail.com

ARTICLE INFO

Article history:
Received: January 7, 2019
Accepted: March 7, 2019
Published: November 20, 2019

Keywords:
1. alachlor
2. atrazine
3. electrochemical degradation
4. DSA
5. ecotoxicity

ABSTRACT: This work studied the electrochemical degradation of alachlor and atrazine (alone and mixed with each other) using a filter-press cell, a dimensionally stable anode (DSA $Ti/Ru_{0.3}Ti_{0.7}O_2$), initial pH 3.0, and temperature at 25 °C. The best operational conditions for alachlor (0.33 mmol L^{-1}) degradation were obtained by a 3^2 factorial design, in which the factors/levels were: NaCl concentration (0.05, 0.1, and 0.15 mol L^{-1}) and current density (10, 30, and 50 mA cm^{-2}). Thus, 93.1% alachlor removal and 71.2% mineralization were achieved using 0.15 mol L^{-1} NaCl and 30 mA cm^{-2}. In addition, the initial degradation products (DPs) of alachlor and atrazine were identified by liquid chromatography coupled to mass spectrometry (LC-MS). Acute and chronic ecotoxicities for three trophic levels (fishes, daphnids and green algae) and lipophilicity (log D, pH 7.4) of the DPs were also estimated using the ECOSAR 1.11 and ChemAxon Calculator software, respectively. The present study showed that the electrochemical degradation is an efficient method for removing the herbicides alachlor and atrazine from water and that the DPs formed have lower pollution potential than their original compounds.

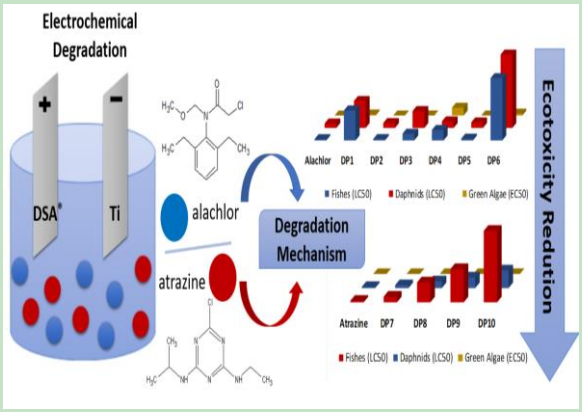

1. Introduction

Alachlor (2-chloro-N-(2,6-diethylphenyl)-N-(methoxymethyl)acetamide) is one of the most frequently used herbicides in weed control, early inhibiting their development. This compound belongs to the chloroacetamide class and it is widely used to protect corn, rice, soybean, peanut, and cotton crops[1]. Alachlor can be degraded by microorganisms present in soils. Therefore, both alachlor and its main metabolite, 2,6-diethylaniline, are ubiquitous in the environment and cause serious ecological and physiological problems[2,3]. Alachlor is a toxic, carcinogenic, persistent organic compound (with a half-life of 70 days in soil and 30 days in water), and an endocrine disruptor[4-7]. The contamination of water resources by alachlor occurs due to runoff and infiltration, causing it to be frequently detected in surface and groundwater samples[8-10].

Atrazine (1-chloro-3-ethylamino-5-isopropylamino-2,4,6-triazine), as well as alachlor, is widely used in weed control in maize, sugarcane, and soybean crops. This herbicide belongs to the triazines group, and it is the most important chemical of this family as well as one of the most used herbicides in the world due to its high phytotoxic activity[11,12]. Among its main characteristics are: low vapor pressure, moderate solubility in water, slow hydrolysis, and the ability of leaching[13,14]. Besides that, atrazine is also a carcinogenic compound and an endocrine

ISSN: 1678-4618
DOI: 10.26850/1678-4618eqj.v44.1SI.2019.p12-25

disruptor. For human consumption, atrazine concentration in water shall not exceed 3 µg L^{-1}. However, higher concentrations are frequently detected in surface and groundwater[15,16].

Alachlor and atrazine are the main active ingredients in many commercial herbicide formulations, which may, in some cases, consist of a mixture of atrazine and alachlor[17]. These formulations have their selective action due to the mixture of the two herbicides that complement each other. The intensive use of these compounds associated with their persistence in the environment and their low biodegradability has contributed to their frequent detection in water. Therefore, it is necessary to develop new methodologies capable of removing those compounds from aqueous systems, since conventional water and sewage treatment plants are inefficient in doing so[18-21].

Among the available methodologies for the treatment of wastewaters containing organic compounds such as alachlor and atrazine, the electrochemical method is very promising. It has been gaining prominence in scientific community due to its versatility, easy automation, high organic removal rate, immobilization of the catalyst in the electrode, and the formation of reactive species on the surface of the electrode[13,22-26].

In electrochemical oxidations, the choice of the material with which the anode is made is of fundamental importance, because the efficiency and selectivity of the process depends on it. Among the most frequently used anodes for the removal of organic compounds is the dimensionally stable anode (DSA) with a nominal composition $Ti/Ru_{0.3}Ti_{0.7}O_2$ [27]. It has been used in the chlor-alkali industry for several years due to its mechanical stability and catalytic activity[28,29]. Several studies report the successful use of the DSA anode[28, 30-34].

The feasibility of a treatment technology should not be assessed only by its potential for degrading a pollutant, but also by the generation of less ecotoxic and more hydrophilic compounds (less prone to bioaccumulation and biomagnification).

Partition coefficients (log P) and distribution coefficients (log D) are the ratios of the concentrations of a compound in a mixture of two immiscible solvents at equilibrium. Log P generally refers to the non-ionized compound, whereas log D refers to the concentration ratio of all species of the compound (ionized and non-ionized). Therefore, the latter coefficient is pH-sensitive. Typically, the most useful pH is 7.4, the physiological one[35,36]. When one of the solvents is water and the other is a nonpolar solvent (usually n-octanol), then those coefficients are a measure of lipophilicity (or hydrophobicity).

Finally, the objective of this work was to study the electrochemical degradation of the herbicides alachlor and atrazine, in a flow cell, using a DSA anode ($Ti/Ru_{0.3}Ti_{0.7}O_2$), assessing the influence of different concentrations of electrolyte and current densities on the removal and mineralization of the organic compounds, besides proposing their respective routes of degradation. The ecotoxicity and lipophilicity of the identified degradation products (DPs) were also estimated.

2. Materials and methods

2.1. Cyclic voltammetry

Cyclic voltammetry (CV) was used to obtain qualitative information about the reaction on the electrode/solution interface. Cyclic voltammograms were obtained using a potentiostat/galvanostat (Autolab, PGSTAT128) and a conventional electrochemical cell composed of: (a) working electrode: circular, dimensionally stable anode plate (DSA) manufactured by De Nora do Brasil Ltda. (nominal composition: $Ti/Ru_{0.3}Ti_{0.7}O_2$; exposed geometric area: 1 cm^2); (b) counter electrode: titanium plate (2 cm^2) parallel to the working electrode; and (c) reference electrode: normal hydrogen electrode (NHE). The assays were performed using 50 mL of 0.05, 0.1, and 0.15 mol L^{-1} NaCl as the supporting electrolyte. Cyclic voltammograms of atrazine and alachlor (both at 0.33 mmol L^{-1}) in NaCl 0.15 mol L^{-1} were also obtained. The potential window was 0.4-1.6 V versus NHE, with scanning speed of 50 mV s^{-1}.

2.2. Electrochemical degradation experiments

The degradation experiments were performed in a filter-press flow-cell using: (a) a commercial DSA $Ti/Ru_{0.3}Ti_{0.7}O_2$ with surface area equal to 14 cm^2 (working electrode); (b) a titanium plate with area equal to 14 cm^2 (counter electrode); (c) a normal hydrogen electrode (NHE) (reference electrode), and (d) a commercial cationic membrane strip (Ionac, MC-3470), immersed in 0.5 mol L^{-1} H_2SO_4, providing the electric contact between the electrochemical cell and the reference electrode (Fig. 1). Besides that, a centrifugal pump

Eclética Química Journal, vol. 44, special issue, 2019, 12-25
ISSN: 1678-4618
DOI: 10.26850/1678-4618eqj.v44.1SI.2019.p12-25

drove the electrolytic solution through the flow-cell. This solution was magnetically stirred.

Initial pH 3, temperature 25 °C, flow rate 130 mL min^{-1} and solution volume 200 mL were held constant throughout the experiments.

Initially, only alachlor (0.33 mmol L^{-1}) was degraded. The experiments followed a 3^2 full factorial design with the central point in triplicate (Statistica 7 software). The studied factors and levels were supporting electrolyte sodium chloride concentration (0.05, 0.1, and 0.15 mol L^{-1}) and current density (10, 30, and 50 mA cm^{-2}).

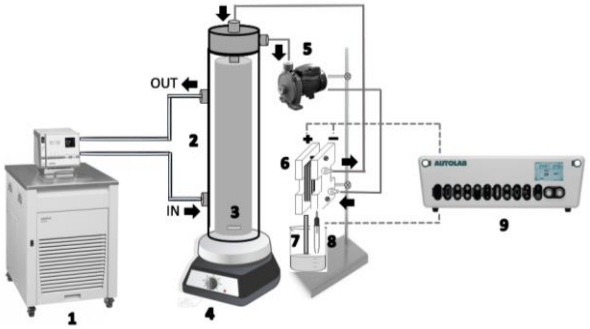

Figure 1. scheme of the experimental apparatus: **1)** Thermostat bath; **2)** reservoir; **3)** magnetic bar; **4)** magnetic stirrer; **5)** centrifugal pump; **6)** flow cell; **7)** cationic membrane; **8)** reference electrode; and **9)** potentiostat/galvanostat.

2.3 Analytical procedures

Total organic carbon analyses (TOC, Shimadzu TOC-VCPH Total Organic Carbon Analyzer) were performed to determine the amount of organic matter in solution, before and after the treatment.

The concentrations of alachlor and atrazine were measured in a high-performance liquid chromatograph (HPLC, Shimadzu LC-10AD VP) equipped with a UV detector (Shimadzu LC-10AVP) and a C_{18} reversed-phase column (Zorbax SB-C_{18}, 5 µm, 25 cm × 4.6 mm). 20 µL were isocratically eluted using a mobile phase composed of acetonitrile and water 70:30 (in volume), flow rate 1 mL min^{-1}, temperature 40 °C and UV detection at 210 nm.

The degradation products (DPs) were identified in a high-performance liquid chromatograph (HPLC, Thermo Scientific Accela 1250 Pump) coupled with a LTQ-Orbitrap Velos spectrometer (HPLC-MS, Thermo Fisher Scientific), operating under the following conditions: positive ion mode electrospray ionization (ESI), electrospray voltage 3.7 kV, nebulization gas pressure 75 psi, heater temperature 500 °C, capillary temperature 400 °C, and injection volume 10 µL. A C_{18} reversed phase column (Zorbax SB-C_{18}, 5 µm, 25 cm × 4.6 mm) and a mobile phase composed of acetonitrile and formic acid 0.1% (70:30 in volume), isocratic mode, and flow rate 1 mL min^{-1} were used.

2.4 Calculations

Ecotoxicities were estimated for three trophic levels (fishes, daphnids and green algae) using the ECOSAR 1.11 software (USEPA, 2017). The acute indicators: LC_{50} (lethal concentration to 50% of the tested organisms) and EC_{50} (effect concentration to 50% of the tested organisms) were estimated. Chronic ecotoxicities were estimated as the geometric mean of the LOEC (lowest-observed-effect concentration) and the NOEC (no-observed-effect concentration). Lipophilicity (log D) values were calculated with the aid of the ChemAxon Calculator.

3. Results and discussion

3.1 Cyclic voltammetry of atrazine and alachlor

Figure 2a shows the cyclic voltammograms of the commercial DSA electrode using NaCl as the supporting electrolyte in the following concentrations: 1) 0.05, 2) 0.1 and 3) 0.15 mol L^{-1}. Figure 2b shows the voltammetric behavior of the commercial DSA electrode with solutions 0.15 mol L^{-1} NaCl in the presence of 4) alachlor (0.33 mmol L^{-1}) and 5) atrazine (0.33 mmol L^{-1}). One can observe that from 0.4 to 1.2 V vs. NHE, no significant increase of the density current occurs; however, for potentials above 1.2 V, there was a fast increase in density current, characterized by the oxygen evolution reaction (OER) and chlorine evolution (Eqs. 1 and 2)[27,29].

$$2\ H_2O \rightarrow O_2 + 4\ H^+ + 4\ e^- \quad (1)$$

$$2\ Cl^- \rightarrow Cl_2 + 2\ e^- \quad (2)$$

Eclética Química Journal, vol. 44, special issue, 2019, 12-25
ISSN: 1678-4618
DOI: 10.26850/1678-4618eqj.v44.1SI.2019.p12-25

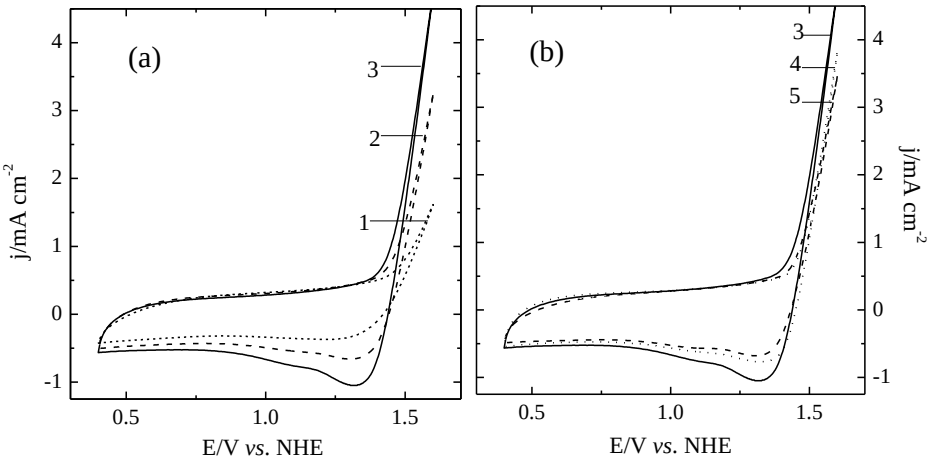

Figure 2. Cyclic voltammograms of the commercial DSA electrode ($Ti/Ru_{0.3}Ti_{0.7}O_2$) recorded between 0.4 and 1.6 V vs. NHE at 50 mV s^{-1} in aqueous solutions containing: (a) 0.05, 0.1, and 0.15 mol L^{-1} NaCl (lines 1, 2, and 3, respectively) and (b) alachlor 0.33 mmol L^{-1} (line 4) and atrazine 0.33 mmol L^{-1} (line 5).

In Figure 2a, it can be observed that oxygen and chlorine evolution reactions became more evident with increasing concentrations of NaCl. However, when the herbicides were added to the 0.15 mol L^{-1} NaCl solution (Fig. 2b), a gradual decrease in current density was noticed for potentials over 1.2 V. That may happen because the adsorption of the herbicides and/or electrogenerated DPs on the anode surface, blocks the electrode active sites[19,30].

3.2 Electrodegradation study

3.2.1 Study of the alachlor electrochemical degradation by factorial design

Table 1 shows the obtained results for alachlor degradation after 120 min of electrolysis (as alachlor was harder to degrade than atrazine, the best operational conditions for the former were also used with the latter).

Table 1. Alachlor removal and mineralization obtained after the electrochemical treatment (3^2 full factorial design with the central point in triplicate).

Experiment	j/mA cm^{-2}	C_{NaCl}/mol L^{-1}	Alachlor removal/%	TOC/%
1	10	0.05	85.0	19.4
2	10	0.10	88.0	20.4
3	10	0.15	89.5	21.7
4	30	0.05	86.5	45.2
5	30	0.10	87.4	70.1
6	30	0.15	93.1	71.2
7	50	0.05	88.0	67.5
8	50	0.10	91.7	70.4
9	50	0.15	93.5	71.6
10	30	0.10	88.0	67.7
11	30	0.10	87.0	68.7
Experimental Error/%			0.5	1.2

ISSN: 1678-4618
DOI: 10.26850/1678-4618eqj.v44.1SI.2019.p12-25

It was possible to assess the effect of the investigated factors on the response-variables (removal evaluated by HPLC and the respective mineralization expressed by TOC values) to determine which of them were statistically significant with a 95% confidence interval (within tested levels). Both factors were significant, and the best tested treatment condition was 0.15 mol L^{-1} NaCl and current density equal to 50 mA cm^{-2}, since the higher the current density and the electrolyte concentration, the higher the removal (93.5%) and the mineralization (71.6%). However, 0.15 mol L^{-1} NaCl and current density equal to 30 mA cm^{-2} were chosen as the actual treatment conditions due to lower electric energy requirements and to the fact that the removal (93.1%) and the mineralization (71.2%) obtained were quite close to the ones at the best tested conditions.

3.2.1.1 Effect of electrolyte concentration and current density

The NaCl concentration affects the production of radicals (and therefore, the oxidation capacity) and current density. These are important parameters for the electrodegradation of any organic compound[30,37].

The obtained results (Table 1) show that increasing current density with a fixed NaCl concentration led to higher removal and mineralization. This same behavior was observed for a fixed current density while increasing the electrolyte concentration. Under all studied conditions, alachlor removals were greater than 80%. However, in none of them the complete removal or mineralization were achieved.

Degradation may take place by two mechanisms: i) the organic compound is adsorbed on the anode surface and then oxidized by anodic electron transfer reaction – direct oxidation; and ii) it reacts with generated active chlorine species with high oxidizing power, according to Eqs. 2, 3 and 4 – indirect oxidation[38,39].

$$Cl_2 + 2H_2O \leftrightarrows HClO + H_3O^+ + Cl^- \quad (3)$$
$$HClO + H_2O \leftrightarrows H_3O^+ + ClO^- \quad (4)$$

Hypochlorous acid (E^o = 1.49 V vs. NHE) act as the main oxidizing agent in the degradation reactions due to its greater oxidation power in comparison to the other electrochemically generated active chlorine species like ClO^- (E^o = 0.89 V vs. NHE) and Cl_2 (1.36 V vs. NHE)[22,40,41]. As the pKa of HClO is 7.5, the protonated species predominates when pH < 7.5. For this reason, all experiments were performed in acidic medium in order to guarantee that the organic compounds were preferably oxidized by HClO, in order to achieve higher rates of removal and mineralization.

Scialdone *et al.*[42] emphasize that intermediates of the OER can react with adsorbed chlorine on the electrode, favoring the oxidation of the organic compound (Eqs. 5 and 6).

$$MO_x(OH) + Cl^- \rightarrow MO_{x+1}(HClO) + e^- \quad (5)$$
$$\text{Organics} + MO_{x+1}(HClO) \rightarrow \text{Intermediates} \rightarrow MO_x + CO_2 + Cl^- + H_2O + H_3O^+ \quad (6)$$

Therefore, increasing sodium chloride concentration increases the formation of electrogenerated chlorine species (Cl_2/HClO/ClO^-) and the use of high current densities leads to an increase in the amount of these species, allowing alachlor degradation[43-45]. For this reason, the highest removal and mineralization of alachlor was achieved with 0.15 mol L^{-1} NaCl and current density equal to 50 mA cm^{-2}. However, regardless of the tested NaCl concentrations and current densities, alachlor mineralization was not complete due to the formation of recalcitrant DPs.

3.2.1.2 Determination of the energy consumption

The electric energy consumption may be estimated by the Electric Energy per Order (EEO in kWh m^{-3} $order^{-1}$). The EEO is defined as the electric energy in kilowatts per hour (kWh) required to degrade a contaminant (C) by one order of magnitude in 1 m^3 (1,000 L) of water or air, as shown in Eq. 7[46-49], where

P = nominal cell power/kW,
t = time/h,
V = volume/L,
C_0 and C_t = initial and final concentrations of the contaminant, respectively.

Eclética Química Journal, vol. 44, special issue, 2019, 12-25
ISSN: 1678-4618
DOI: 10.26850/1678-4618eqj.v44.1SI.2019.p12-25

It is important to notice that Eq. 7 is multiplied by 1,000 to convert volume from L into m^{-3} and that it can only be used if the chemical reaction follows a pseudo-first order kinetics, as was the case of alachlor[8].

$$E_{EO}(kWh\,m^{-3}\,order^{-1}) = \frac{P \times t \times 1000}{V \times \log(C_0/C_t)} \qquad (7)$$

According to Thiam *et al.*[50], the energy consumption can also be expressed per unit of TOC mass, as shown in Eq. 8, where

E_{cell} = average cell voltage (V),
I = applied current (A),
t = electrolysis time (h),
V = volume (L), and
$\Delta(TOC)exp$ is the observed TOC decrease (mg L^{-1}).

$$EC_{TOC}\ (kWh\ g_{TOC}{}^{-1}) = \frac{E_{cell} \times I \times t}{V \times \Delta(TOC)_{exp}} \qquad (8)$$

Figure 3 shows E_{EO} and EC_{TOC} as a function of the applied current density, calculated for the alachlor degradation experiments. In Fig. 3a, one can notice that, for a fixed current density, as the NaCl concentration increases, energy consumption decreases. This is because the conductivity of the medium also increases, decreasing cell potential, which leads to lower values of energy consumption, as previously described[28,44]. In addition, for the same concentration of the supporting electrolyte, there is a concomitant increase in energy consumption, due to the cell operational potential increase and the competition between O_2 and Cl_2 formation at higher potential values[44]. Comparing Fig. 3a and 3b, one can observe that the behavior of the energy consumption calculated by Eq. 8 is very similar.

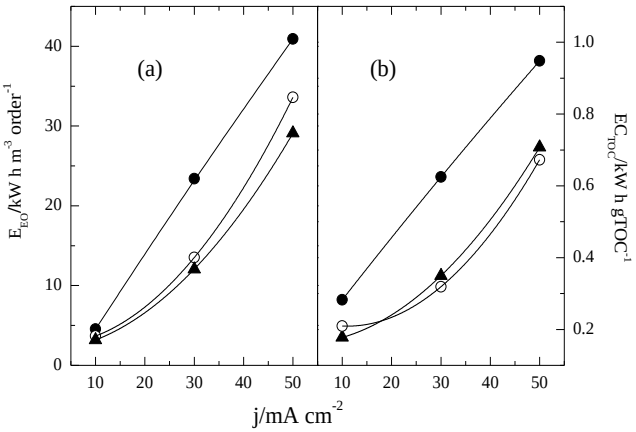

Figure 3. Dependence of energy consumption (kWh m^{-3} $order^{-1}$ and kWh $g_{TOC}{}^{-1}$) with applied current density in NaCl solution: (●) 0.05, (○) 0.10 and (▲) 0.15 mol L^{-1}. Electrolysis performed using a commercial $Ti/Ru_{0.3}Ti_{0.7}O_2$ DSA anode.

3.2.2 Electrochemical degradation of atrazine and alachlor-atrazine mixture

Some of the major companies producing agrochemicals trade alachlor in mixture with atrazine as a way to enhance the action of both herbicides. One of the usual compositions is the ratio of 1:1 (in volume) and, for this reason, the mixture employed in the present work was composed of 0.33 mmol L^{-1} of each substance.

One can observe that atrazine was removed after 45 min of electrolysis (Fig. 4), while alachlor took more than 120 min of treatment to reach a similar degradation.

Eclética Química Journal, vol. 44, special issue, 2019, 12-25
ISSN: 1678-4618
DOI: 10.26850/1678-4618eqj.v44.1SI.2019.p12-25

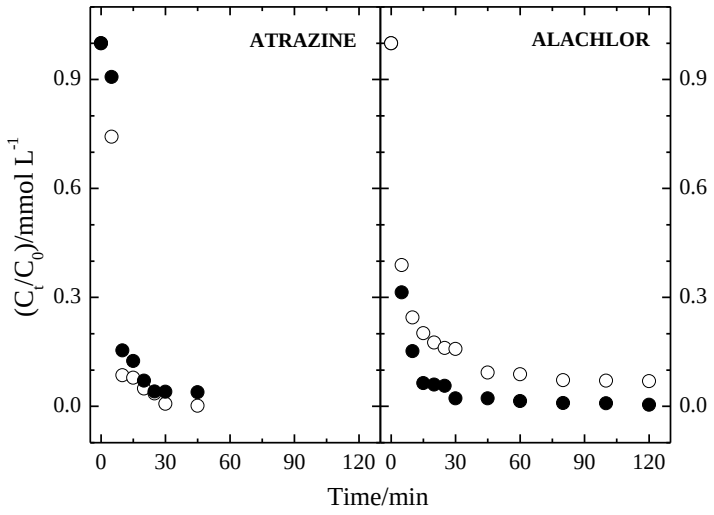

Figure 4. Variation of atrazine and alachlor concentrations with treatment time: (○) alone and (●) in the mixture.

Energy consumption, TOC, and obtained removals are given in Table 2. One can observe that alachlor alone required more energy to be degraded. In none of the applied conditions the complete mineralization of the compounds was achieved, which can be attributed to the formation of recalcitrant DPs during electrolysis.

Another finding is that, apparently, there is some kind of synergism between alachlor and atrazine. When those two substances were degraded together, alachlor removal and, mainly its mineralization, were increased. Also, energy consumption significantly decreased. The reasons for that behavior are not yet understood. However, that it is a true advantage, as alachlor and atrazine are usually employed together.

Table 2. Results obtained for the removals of alachlor, atrazine and their mixture, mineralization, and energy consumption estimated after electrochemical degradation (120 min, 30 mA cm^{-2}, and 0.15 mol L^{-1} NaCl).

Compound	Removal/%	TOC/%	E_{EO}/ kWh m^{-3} $order^{-1}$	EC_{TOC}/kWh g_{TOC}^{-1}
Alachlor only	93.1	71.0	12.1	0.35
Atrazine only	100	70.4	5.0	0.20
Alachlor-Atrazine (1:1)	99.6 100	82.8	7.1	0.22

3.3 Alachlor electrochemical degradation mechanism proposition

Fig. 5 shows a proposition for the alachlor electrochemical degradation route. The m/z ratios here refer to the compounds in their protonated form, $[M+H]^+$. Initially, the molecular ion that characterizes alachlor was identified with m/z = 270. Partial oxidative cleavage of the bond in the $-OCH_3$ group connected to N, followed by dehalogenation and subsequent hydroxylation leads to the formation of the DP with m/z = 222. This compound also was identified by Pipi *et al.*[8] and Wang and Zhang[51]. In addition, this DP was also detected in water samples in Massachusetts[3].

According to Pipi *et al.*[8], the formation of the DP with m/z = 284 is characterized by a purely oxidative mechanism due to hydroxyl radicals. Hydroxyl radicals can also convert lipophilic into

ISSN: 1678-4618
DOI: 10.26850/1678-4618eqj.v44.1SI.2019.p12-25

hydrophilic compounds. That is, from the structural point of view, the DP with m/z = 284 is more soluble in water than its parent compound due to an increased number of polar groups in its structure[6]. The subsequent demethylation followed by the addition of H^+ leads to the formation of another DP with m/z = 270[8,51]. DPs with m/z = 158, 176, and 224 were also identified in this work. These compounds are quinoline and indoline derivatives, obtained by the complex cleavage of certain bonds followed by cyclization[8,52].

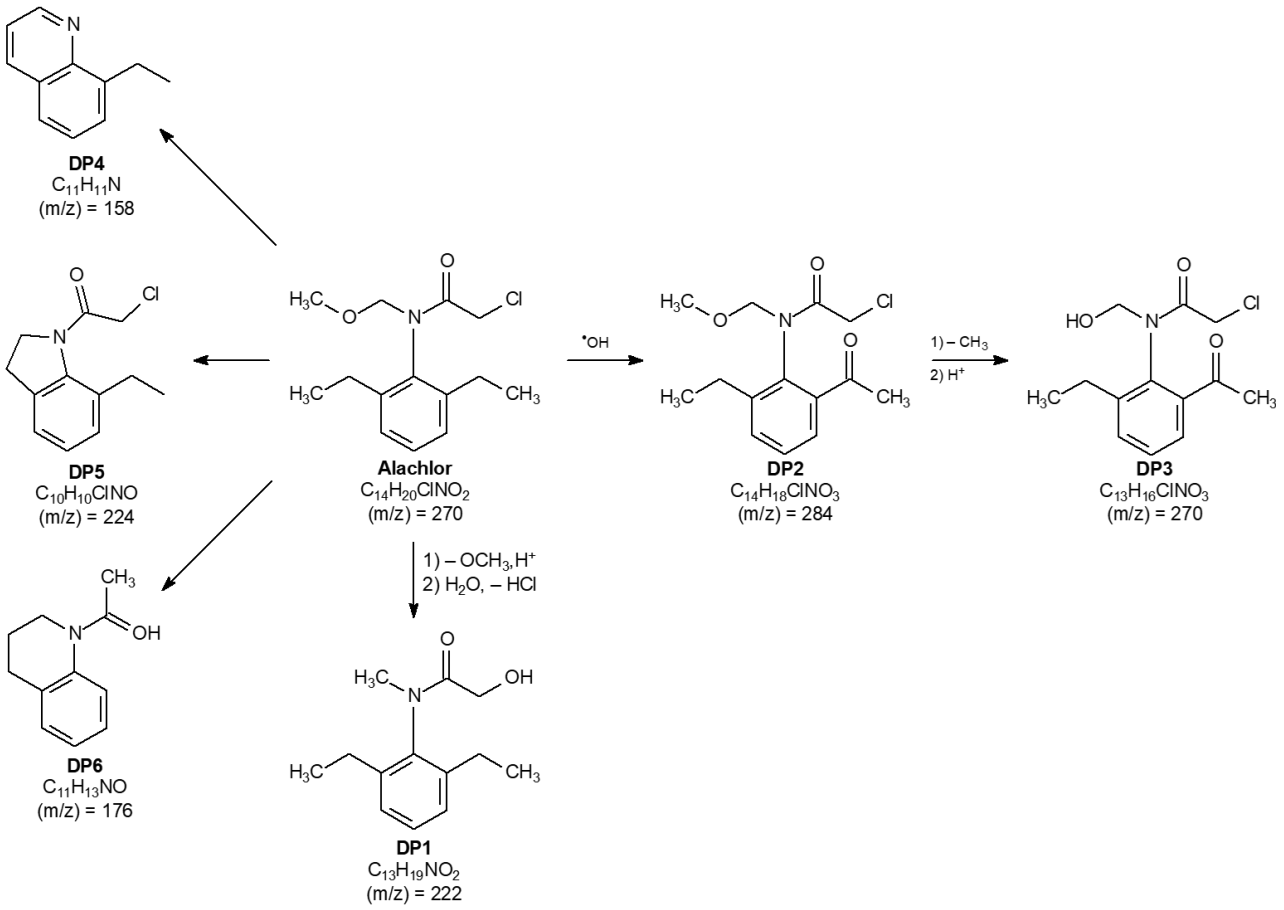

Figure 5. Proposition of the initial mechanism for the electrochemical degradation of alachlor using a commercial $Ti/Ru_{0.3}Ti_{0.7}O_2$ DSA anode in aqueous medium containing 0.15 mol L^{-1} NaCl.

3.4 Atrazine electrochemical degradation mechanism proposition

Fig. 6 shows a proposition for the atrazine electrochemical degradation route. The m/z ratios of the structures also correspond to the protonated forms, $[M+H]^+$.

The molecular ion of atrazine has m/z = 216. Dechlorination of atrazine followed by hydroxylation led to the formation of the DP with m/z = 198. This is the main degradation product of atrazine[53]. According to Chen, Yang *et al*[54], the C–Cl bond in atrazine is the lengthiest one, approximately 1.73 Å, making it easier to undergo some sort of cleavage. The subsequent deamination with the total loss of the side chain ($–NHCH_2CH_3$), followed by hydroxylation forms the DP with m/z = 171[48,54].

Two other DPs were identified. The first one, with m/z = 218, was formed by atrazine demethylation followed by hydroxylation. The DP with m/z = 232 was formed due to the abstraction of a hydrogen atom followed by hydroxylation.

ISSN: 1678-4618
DOI: 10.26850/1678-4618eqj.v44.1SI.2019.p12-25

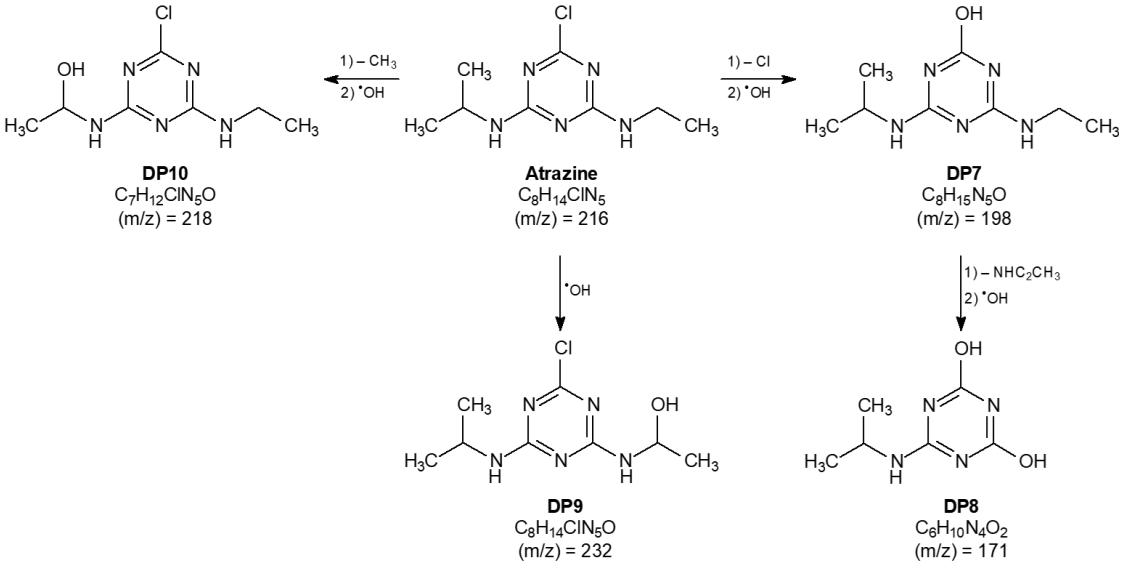

Figure 6. Proposition of the initial mechanism for the electrochemical degradation of atrazine using a commercial $Ti/Ru_{0.3}Ti_{0.7}O_2$ DSA anode in aqueous medium containing 0.15 mol L^{-1} NaCl.

3.5 Lipophilicity and ecotoxicity of alachlor, atrazine, and their degradation products

The distribution coefficients (log D, pH 7.4) of alachlor, atrazine, and their degradation products (DPs) are presented in Fig. 7.

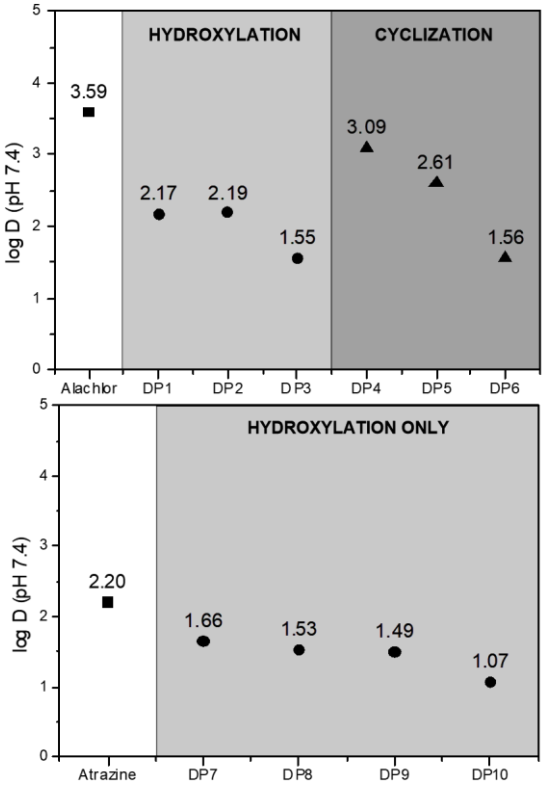

Figure 7. Calculated lipophylicity (log D at pH 7.4) of alachlor, atrazine, and their degradation products.

It is possible to observe that alachlor and its DPs have log D > 0. This is an indication that those compounds preferentially dissolve in non-polar media, representing a risk factor for living beings due to their bioaccumulation potential. The log D of all alachlor DPs are smaller than that of alachlor (3.59) due to the insertion of polar groups into their structures during electrolysis, which contribute to the increase in their aqueous solubility, and to smaller carbon chains compared to alachlor.

Among alachlor DPs, those formed by hydroxylation produced, in average, DPs with lower lipophilicity. DP3 is the compound with the lowest calculated lipophilicity (log D ≅ 1.55), due to the insertion of a carbonyl in one of the ethyl groups bonded to the aromatic ring and to the replacement of a methoxy group by a hydroxyl one, in one of the carbon chains bonded to the nitrogen atom. Its log D is twice as lower as that of alachlor.

In relation to the DPs formed by cyclization, from DP4 (3.09) to DP5 (2.61), log D decreases by one order of magnitude, due to the loss of aromaticity in one of the rings. From DP5 (2.61) to DP6 (1.56), log D decreases another order of magnitude, due to the loss of the ethyl group bonded to the aromatic ring and dechlorination. DP3 and DP6 have similar lipophilicities.

The lipophilicity of atrazine (2.20) is an order of magnitude lower than that of alachlor (3.59). Atrazine and its DPs have also log D > 0, indicating that their preferably dissolve in non-polar media. The log D of all atrazine DPs are smaller than that

Eclética Química Journal, vol. 44, special issue, 2019, 12-25
ISSN: 1678-4618
DOI: 10.26850/1678-4618eqj.v44.1SI.2019.p12-25

of atrazine, in average one order of magnitude lower. The chemical features that make those compounds more water-soluble compared to atrazine are the smaller carbon chains and the increased number of polar groups in their structures.

Figure 8 shows the estimated acute and chronic ecotoxicities for freshwater organisms at three trophic levels (fishes, daphnids and green algae) of alachlor, atrazine and their DPs. It is important to observe that acute toxicity is usually observed within the first 24-48 h after exposure to the deleterious substance(s), whereas the chronic one is later observed (sometimes weeks or months after the exposure). In this context, the lower the concentration of those compounds that causes harmful effects, the greater their ecotoxicity.

Alachlor acute and chronic estimated ecotoxicities were high for all tested organisms (fishes, daphnids and green algae) (Fig. 8). This could be attributed to: (i) alachlor is a compound with high log D value (3.59), which is an indication of its ability to dissolve in fat tissues of animals (fishes and daphnids) and (ii) as alachlor is a herbicide, whose main function is to prevent photosynthesis from happening, it is expected to be quite toxic to green algae. Approximately, the DPs formed from alachlor are equally toxic to fishes and daphnids. That is probably because all degradation products, as well as alachlor, have high lipophilicity.

Among the DPs formed from alachlor, the least toxic is DP6, which is the compound that presented the lowest lipophilicity. Therefore, increased concentrations of those compounds are necessary to harm fishes and daphnids, since they are easier to be eliminated by the organisms. Alachlor is much more toxic than atrazine (16, 4 and 26 times more toxic to fishes, daphnids and green algae, respectively).

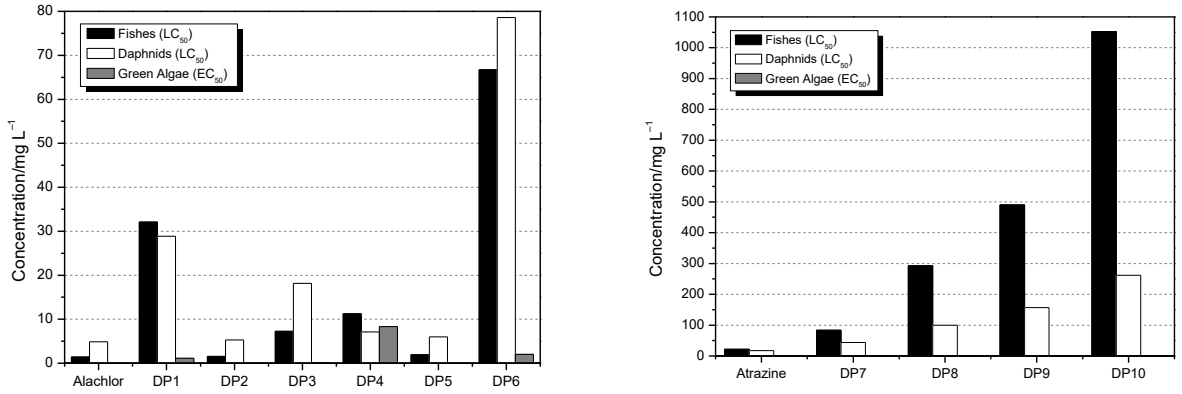

(a) Acute ecotoxicity

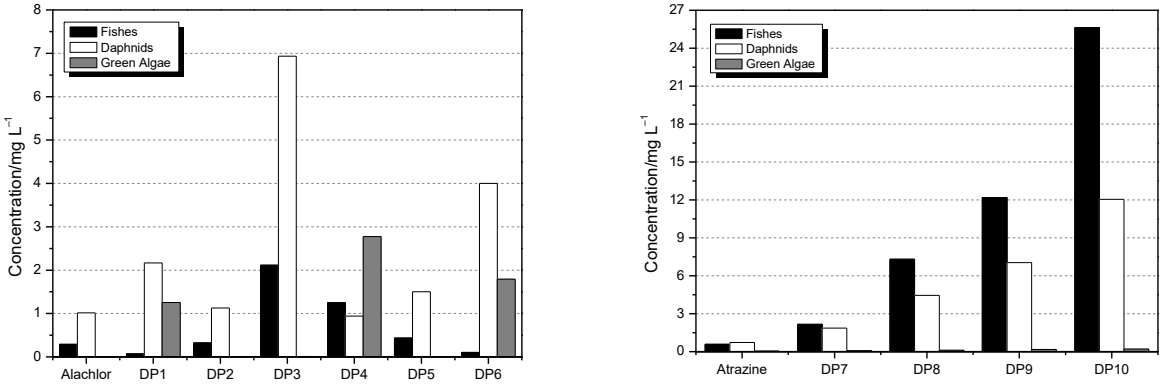

(b) Chronic ecotoxicity

Figure 8. Estimated acute and chronic ecotoxicities of alachlor, atrazine, and their degradation products, using the ECOSAR 1.11 software (USEPA), for three trophic levels: fishes, daphnids and green algae. Chronic ecotoxicities are the geometric mean between the lowest-observed-effect concentration (LOEC) and the no-observed-effect concentration (NOEC).

Eclética Química Journal, vol. 44, special issue, 2019, 12-25
ISSN: 1678-4618
DOI: 10.26850/1678-4618eqj.v44.1SI.2019.p12-25

Atrazine and its DPs also have high acute ecotoxicities towards green algae due to their herbicidal action, preventing photosynthesis to happen. The atrazine DPs are less toxic to daphnids and fishes compared to atrazine, in the order DP7 > DP8 > DP9 > DP10. This may be ascribed to the partition coefficients of these compounds, which are lower than that of atrazine, making it necessary to increase the DPs concentration to cause fishes and daphnids mortality. In addition, all of atrazine DPs are more toxic to daphnids than to fishes.

Over time, the difference between the ecotoxicities of alachlor and atrazine decreased, so that their chronic ecotoxicities are similar. In addition, it is possible to observe that alachlor (atrazine) concentrations that cause chronic ecotoxicity are on average 10 (40) times lower than those that cause acute ecotoxicity. It is important to emphasize that atrazine and corresponding DPs ecotoxicity profile is quite similar, whether acute or chronic ecotoxicities are considered.

4. Conclusions

The DSA in the presence of chloride, led to high removals of alachlor and atrazine due to the formation of active chlorine species with high oxidant power (Cl_2/HOCl/ClO^-) and the generation of chemically adsorbed hydroxyl radicals on the surface of the electrode. However, in none of the experiments, it was possible to achieve complete mineralization of the organic compounds, due to the formation of recalcitrant DPs (some of which were identified in this work) and to the short electrolysis time (120 min).

The identified DPs of alachlor and atrazine in this work have already been reported in the literature; however, the electrolysis was performed under different conditions. Based on the structures of the DPs identified in this work, it was possible to estimate their acute and chronic ecotoxicities towards three different trophic levels (fishes, daphnids and green algae) and their distribution coefficients (log D). Those parameters allow one to conclude that all formed DPs have lower pollution potential than their original compounds, although they still pose threats to the environment.

In this context, the present study showed that the electrochemical degradation is effective and can be used for the treatment of residues of pesticides in formulations containing alachlor and atrazine.

References

[1] Słaba, M., Różalska, S., Bernat, P., Szewczyk, R., Piątek, M. A., Długoński, J., Efficient alachlor degradation by the filamentous fungus *Paecilomyces marquandii* with simultaneous oxidative stress reduction, Bioresource Technology 197 (Supplement C) (2015) 404-409. https://doi.org/10.1016/j.biortech.2015.08.045.

[2] Pérez, M. H., Vega, L. P., Zúñiga-Benítez, H., Peñuela, G. A., Comparative Degradation of alachlor using photocatalysis and photo-Fenton, Water, Air, & Soil Pollution 229 (11) (2018) 346. https://doi.org/10.1007/s11270-018-3996-6.

[3] Potter, T. L., Carpenter, T. L., Occurrence of alachlor environmental degradation products in groundwater, Environmental Science & Technology 29 (6) (1995) 1557-1563. https://doi.org/10.1021/es00006a018.

[4] United States Environmental Protection Agency, Registration eligibility decision (RED) alachlor, 1998. https://archive.epa.gov/pesticides/reregistration/web/pdf/0063.pdf.

[5] Chen, C. Z., Yan, C. T., Kumar, P. V., Huang, J. W., Jen, J. F., Determination of alachlor and its metabolite 2,6-diethylaniline in microbial culture medium using online microdialysis enriched-sampling coupled to high-performance liquid chromatography, Journal of Agricultural and Food Chemistry 59 (15) (2011) 8078-8085. https://doi.org/10.1021/jf201129j.

[6] Kidak, R., Dogan, S., Degradation of trace concentrations of alachlor by medium frequency ultrasound, Chemical Engineering and Processing: Process Intensification 89 (Supplement C) (2015) 19-27. https://doi.org/10.1016/j.cep.2014.12.010.

[7] Mello, R., Santos, L. H. E., Pupo, M. M. S., Eguiluz, K. I. B., Salazar-Banda, G. R., Motheo, A. J., Alachlor removal performance of Ti/$Ru_{0.3}Ti_{0.7}O_2$ anodes prepared from ionic liquid solution, Journal of Solid State Electrochemistry 22 (5) (2018) 1571-1580. https://doi.org/10.1007/s10008-017-3700-6.

[8] Pipi, A. R. F., Andrade, A. R., Brillas, E., Sirés, I., Total removal of alachlor from water by electrochemical processes, Separation and Purification Technology 132 (Supplement C) (2014) 674-683. https://doi.org/10.1016/j.seppur.2014.06.022.

[9] Sánchez-Camazano, M., Lorenzo, L. F., Sánchez-Martín, M. J., Atrazine and alachlor inputs to surface and ground waters in irrigated corn cultivation areas of castilla-leon region, Spain, Environmental Monitoring and Assessment 105 (1) (2005) 11-24. https://doi.org/10.1007/s10661-005-2814-y.

ISSN: 1678-4618
DOI: 10.26850/1678-4618eqj.v44.1SI.2019.p12-25

[10] Spalding, R. F., Exner, M. E., Snow, D. D., Cassada, D. A., Burbach, M. E., Monson, S. J., Herbicides in ground water beneath Nebraska's management systems evaluation area, Journal of Environmental Quality 32 (1) (2003) 92-99. https://doi.org/10.2134/jeq2003.0092.

[11] Guan, S. H., Huang, M. W., Li, X. P., Cai, Q., Determination of atrazine, simazine, alachlor, and metolachlor in surface water using dispersive pipette extraction and gas chromatography-mass spectrometry, Analytical Letters 51 (4) (2018) 613-625. https://doi.org/10.1080/00032719.2017.1341904.

[12] Leal, D. P. B., Dick, D. P., Stahl, A. M., Köppchen, S., Burauel, P., Atrazine degradation patterns: the role of straw cover and herbicide application history, Scientia Agricola 76 (2019) 63-71. https://doi.org/10.1590/1678-992x-2017-0230.

[13] Aquino, J. M., Miwa, D. W., Rodrigo, M. A., Motheo, A. J., Treatment of actual effluents produced in the manufacturing of atrazine by a photo-electrolytic process, Chemosphere 172 (Supplement C) (2017) 185-192. https://doi.org/10.1016/j.chemosphere.2016.12.154.

[14] Santana, H., Bonancea, C. E., Takashima, K., Photoelectrochemical degradation of atrazina on titanium dioxide: Effect of different experimental parameters, Química Nova 26 (6) (2003) 807-811. https://doi.org/10.1590/s0100-40422003000600005.

[15] United States Environmental Protection Agency, Decision documents for atrazine. 2006. https://swap.stanford.edu/20120106041942/http://www.epa.gov/oppsrrd1/REDs/atrazine_combined_docs.pdf.

[16] Hladik, M. L., Bouwer, E. J., Roberts, A. L., Neutral degradates of chloroacetamide herbicides: Occurrence in drinking water and removal during conventional water treatment, Water Research 42 (20) (2008) 4905-4914. https://doi.org/10.1016/j.watres.2008.09.008.

[17] Henriet, M. M., Mitchell, R. W., Prill, E. J., Emulsion flowable formulation containing a mixture of alachlor/atrazine as the active agent: Google Patents 1989. https://patents.google.com/patent/EP0142485B1/en.

[18] Gomes, F. E. R., Souza, N. E., Galinaro, C. A., Arriveti, L. O. R., Assis, J. B., Tremiliosi-Filho, G., Electrochemical degradation of butyl paraben on platinum and glassy carbon electrodes, Journal of Electroanalytical Chemistry 769 (2016) 124-130. https://doi.org/10.1016/j.jelechem.2016.03.016.

[19] Souza, F. L., Aquino, J. M., Miwa, D. W., Rodrigo, M. A., Motheo, A. J., Electrochemical degradation of dimethyl phthalate ester on a DSA® electrode, Journal of the Brazilian Chemical Society 25 (3) (2014) 492-501. https://doi.org/10.5935/0103-5053.20140007.

[20] Zheng, D., Xin, Y. J., Ma, D., Wang, X., Wu, J., Gao, M. C., Preparation of graphene/TiO_2 nanotube array photoelectrodes and their photocatalytic activity for the degradation of alachlor, Catalysis Science & Technology 6 (6) (2016) 1892-1902. https://doi.org/10.1039/c5cy00887e.

[21] Wardenier, N., Vanraes, P., Nikiforov, A., Van Hulle, S. W. H., Leys, C., Removal of micropollutants from water in a continuous-flow electrical discharge reactor, Journal of Hazardous Materials 362 (2019) 238-245. https://doi.org/10.1016/j.jhazmat.2018.08.095.

[22] Fornazari, A. L. T., Malpass, G. R. P., Miwa, D. W., Motheo, A. J., Application of electrochemical degradation of wastewater composed of mixtures of phenol-formaldehyde, Water Air and Soil Pollution 223 (8) (2012) 4895-4904. https://doi.org/10.1007/s11270-012-1245-y.

[23] Malpass, G. R. P., Miwa, D. W., Santos, R. L., Vieira, E. M., Motheo, A. J., Unexpected toxicity decrease during photoelectrochemical degradation of atrazine with NaCl, Environmental Chemistry Letters 10 (2) (2012) 177-182. https://doi.org/10.1007/s10311-011-0340-4.

[24] Malpass, G. R. P., Salazar-Banda, G. R., Miwa, D. W., Machado, S. A. S., Motheo, A. J., Comparing atrazine and cyanuric acid electro-oxidation on mixed oxide and boron-doped diamond electrodes, Environmental Technology 34 (8) (2013) 1043-1051. https://doi.org/10.1080/09593330.2012.733420.

[25] Rajeshwar, K., Ibanez, J. G., Swain, G. M., Electrochemistry and the environment. Journal of Applied Electrochemistry 24 (11) (1994) 1077-1091. https://doi.org/10.1007/BF00241305.

[26] Pieczyńska, A., Ossowski, T., Bogdanowicz, R., Siedlecka, E., Electrochemical degradation of textile dyes in a flow reactor: effect of operating conditions and dyes chemical structure, International Journal of Environmental Science and Technology 16 (2) (2019) 929-942. https://doi.org/10.1007/s13762-018-1704-0.

[27] Pinto, C. F., Antonelli, R., Araújo, K. S., Fornazari, A. L. T., Fernandes, D. M., Granato, A. C., Azevedo, E. B., Malpass, G. R. P., Experimental-design-guided approach for the removal of atrazine by sono-electrochemical-UV-chlorine techniques, Environmental Technology 40 (4) (2019) 430-440. https://doi.org/10.1080/09593330.2017.1395480.

[28] Malpass, G. R. P., Miwa, D. W., Mortari, D. A., Machado, S. A. S., Motheo, A. J., Decolorisation of real textile waste using electrochemical techniques: Effect of the chloride concentration, Water Research 41 (13) (2007) 2969-2977. https://doi.org/10.1016/j.watres.2007.02.054.

[29] Parra, K. N., Gul, S., Aquino, J. M., Miwa, D. W., Motheo, A. J., Electrochemical degradation of tetracycline in artificial urine medium, Journal of Solid State Electrochemistry 20 (4) (2016) 1001-1009. https://doi.org/10.1007/s10008-015-2833-8.

[30] Hussain, S., Gul, S., Steter, J. R., Miwa, D. W., Motheo, A. J., Route of electrochemical oxidation of the antibiotic sulfamethoxazole on a mixed oxide anode, Environmental Science and Pollution Research 22 (19) (2015) 15004-15015. https://doi.org/10.1007/s11356-015-4699-9.

[31] Malpass, G. R. P., Miwa, D. W., Gomes, L., Azevedo, E. B., Vilela, W. F. D., Fukunaga, M. T., Guimaraes, J. R., Bertazzoli, R., Machado, S. A. S., Motheo, A. J., Photo-assisted electrochemical degradation of the commercial herbicide atrazine, Water Science and Technology 62 (12) (2010) 2729-2736. https://doi.org/10.2166/wst.2010.207.

[32] Malpass, G. R. P., Miwa, D. W., Machado, S. A. S., Motheo, A. J., SnO_2-based materials for pesticide degradation, Journal of Hazardous Materials 180 (1-3) (2010) 145-151. https://doi.org/10.1016/j.jhazmat.2010.04.006.

[33] Montes, I. J. S., Silva, B. F., Aquino, J. M., On the performance of a hybrid process to mineralize the herbicide tebuthiuron using a DSA® anode and UVC light: A mechanistic study, Applied Catalysis B-Environmental 200 (2017) 237-245. https://doi.org/10.1016/j.apcatb.2016.07.003.

[34] Santos, T. E. S., Silva, R. S., Meneses, C. T., Martinez-Huitle, C. A., Eguiluz, K. I. B., Salazar-Banda, G. R., Unexpected enhancement of electrocatalytic nature of Ti/(RuO_2)(x)-(Sb_2O_5)(y) anodes prepared by the ionic liquid-thermal decomposition method, Industrial & Engineering Chemistry Research 55 (11) (2016) 3182-3187. https://doi.org/10.1021/acs.iecr.5b04690.

[35] Bharate, S. S., Kumar, V., Vishwakarma, R. A., Determining partition coefficient (Log P), distribution coefficient (Log D) and ionization constant (pKa) in early drug discovery, Combinatorial Chemistry & High Throughput Screening 19 (6) (2016) 461-469. https://doi.org/10.2174/1386207319666160502123917.

[36] Csizmadia, F., Tsantili-Kakoulidou, A., Panderi, I., Darvas, F., Prediction of distribution coefficient from structure .1. Estimation method, Journal of Pharmaceutical Sciences 86 (7) (1997) 865-871. https://doi.org/10.1021/js960177k.

[37] Zhang, H., Liu, F., Wu, X. G., Zhang, J. H., Zhang, D. B., Degradation of tetracycline in aqueous medium by electrochemical method, Asia-Pacific Journal of Chemical Engineering 4 (5) (2009) 568-573. https://doi.org/10.1002/apj.286.

[38] Rajkumar, D., Kim, J. G., Oxidation of various reactive dyes with *in situ* electro-generated active chlorine for textile dyeing industry wastewater treatment, Journal of Hazardous Materials 136 (2) (2006) 203-212. https://doi.org/10.1016/j.hazement.2005.11.096.

[39] Trasatti, S., Electrocatalysis: understanding the success of DSA®, Electrochimica Acta 45 (15-16) (2000) 2377-2385. https://doi.org/10.1016/s0013-4686(00)00338-8.

[40] Cheng, C. Y., Kelsall, G. H., Models of hypochlorite production in electrochemical reactors with plate and porous anodes, Journal of Applied Electrochemistry 37 (11) (2007) 1203-1217. https://doi.org/10.1007/s10800-007-9364-7.

[41] Pipi, A. R. F., Aquino Neto, S., Andrade, A. R., Electrochemical degradation of diuron in chloride medium using DSA® based anodes, Journal of the Brazilian Chemical Society 24 (8) (2013) 1259-1266. https://doi.org/10.5935/0103-5053.20130159.

[42] Scialdone, O., Randazzo, S., Galia, A.,Silvestri, G., Electrochemical oxidation of organics in water: Role of operative parameters in the absence and in the presence of NaCl, Water Research 43 (8) (2009) 2260-2272. https://doi.org/10.1016/j.watres.2009.02.014.

[43] Chauhan, R., Srivastava, V. C., Hiwarkar, A. D., Electrochemical mineralization of chlorophenol by ruthenium oxide coated titanium electrode, Journal of the Taiwan Institute of Chemical Engineers 69 (2016) 106-117. https://doi.org/10.1016/j.jtice.2016.10.016.

[44] Gomes, L., Miwa, D. W., Malpass, G. R. P., Motheo, A. J., Electrochemical degradation of the dye reactive orange 16 using electrochemical flow-cell, Journal of the Brazilian Chemical Society 22 (7) (2011) 1299-1306. https://doi.org/10.1590/s0103-50532011000700015.

[45] Hussain, S., Steter, J. R., Gul, S.,Motheo, A. J., Photo-assisted electrochemical degradation of sulfamethoxazole using a Ti/$Ru_{0.3}Ti_{0.7}O_2$ anode: Mechanistic and kinetic features of the process, Journal of Environmental Management 201 (2017) 153-162. https://doi.org/10.1016/j.jenvman.2017.06.043.

[46] Bessegato, G. G., Cardoso, J. C., Silva, B. F., Zanoni, M. V. B., Combination of photoelectrocatalysis and ozonation: A novel and powerful approach applied in acid yellow 1 mineralization, Applied Catalysis B-Environmental 180 (2016) 161-168. https://doi.org/10.1016/j.apcatb.2015.06.013.

[47] Bolton, J. R., Bircher, K. G., Tumas, W., Tolman, C. A., Figures-of-merit for the technical development and application of advanced oxidation technologies for both electric- and solar-driven systems (IUPAC Technical Report), Pure and Applied Chemistry 73 (4) (2001) 627-637. https://doi.org/10.1351/pac200173040627.

[48] Khan, J. A., He, X., Shah, N. S., Khan, H. M., Hapeshi, E., Fatta-Kassinos, D., Dionysiou, D. D., Kinetic and mechanism investigation on the photochemical degradation of atrazine with activated H_2O_2, $S_2O_8^{2-}$ and HSO_5, Chemical Engineering Journal 252 (2014) 393-403. https://doi.org/10.1016/j.cej.2014.04.104.

[49] Malpass, G. R. P., Miwa, D. W., Machado, S. A. S., Motheo, A. J., Decolourisation of real textile waste using electrochemical techniques: Effect of electrode composition, Journal of Hazardous Materials 156 (1-3) (2008) 170-177. https://doi.org/10.1016/j.jhazmat.2007.12.017.

[50] Thiam, A., Salazar, R., Brillas, E., Sirés, I., Electrochemical advanced oxidation of carbofuran in aqueous sulfate and/or chloride media using a flow cell with a RuO_2-based anode and an air-diffusion cathode at pre-pilot scale, Chemical Engineering Journal 335 (2018) 133-144. https://doi.org/10.1016/j.cej.2017.10.137.

[51] Wang, X. K., Zhang, Y., Degradation of alachlor in aqueous solution by using hydrodynamic cavitation, Journal of Hazardous Materials 161 (1) (2009) 202-207. https://doi.org/10.1016/j.jhazmat.2008.03.073.

[52] Qiang, Z. M., Liu, C., Dong, B. Z., Zhang, Y. L., Degradation mechanism of alachlor during direct ozonation and O_3/H_2O_2 advanced oxidation process, Chemosphere 78 (5) (2010) 517-526. https://doi.org/10.1016/j.chemosphere.2009.11.037.

[53] Javaroni, R. D. A., Landgraf, M. D., Rezende, M. O. O., Behavior of the herbicides atrazine and alachlor after application on soils prepared to sugar cane plantation, Química Nova 22 (1) (1999) 58-64. http://doi.org/10.1590/S0100-40421999000100012.

[54] Chen, C., Yang, S. G., Guo, Y. P., Sun, C., Gu, C. G., Xu, B., Photolytic destruction of endocrine disruptor atrazine in aqueous solution under UV irradiation: Products and pathways, Journal of Hazardous Materials 172 (2-3) (2009) 675-684. https://doi.org/10.1016/j.jhazmat.2009.07.050.

Eclética Química Journal

Original article
iq.unesp.br/ecletica

| Vol. 44 | special issue | 2019 |

Electrodeposition study of the Cu-Zn-Mo system in citrate/sulfate medium

Hugo Sousa Santos[1], Alessandra Alves Correa[1], Murilo Fernando Gromboni[2], Lucia Helena Mascaro[1+]

1.Federal University of São Carlos (UFSCar), Department of Chemistry, Km 235 Washington Luís Hw, São Carlos, São Paulo, Brazil
2.University of São Paulo (USP), Institute of Chemistry, 400 Trabalhador São Carlense Ave, São Carlos, São Paulo, Brazil

[+]Corresponding author: Lucia Helena Mascaro, phone: +55 16 33519698, email address: lmascaro@ufscar.br

ARTICLE INFO

Article history:
Received: January 16, 2019
Accepted: August 3, 2019
Published: November 20, 2019

Keywords:
1. electrodeposition
2. Cu-Zn-Mo system
3. composite
4. alloy
5. intermetallic phases
6. molybdenum oxides

ABSTRACT: Alloys and composites that contain molybdenum have been studied due to their excellent properties, such as corrosion resistance and catalytic activity. In this work, the parameters for Cu-Zn-Mo system electrodeposition were studied, such as deposition potentials and concentration of electroactive species. The deposition potentials were examined using cyclic voltammetry and anodic linear stripping voltammetry (ALSV), the deposit morphology was evaluated using scanning electron microscopy (SEM) and crystallographic characterization was carried out for X-ray diffraction (XRD). The voltammetry studies indicated co-deposition of the metals in potentials more negative than -1.2 V, and a potential deposition at -1.5 V was chosen. The coatings presented morphology compact with small agglomerated particles with cauliflower structures, and the content of molybdenum, copper, and zinc ranged from 5 to 8%, 30 to 40% and 20 to 28%, respectively.

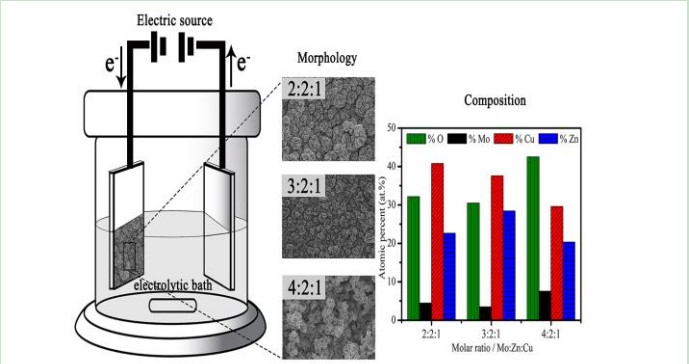

The Mo-Zn-Cu system electrodeposition was studied. The coatings had cauliflower morphology and the content Mo, Cu and Zn ranged from 5 to 8%, 30 to 40% and 20 to 28%, respectively.

1. Introduction

Alloys and composites of zinc (Zn) and copper (Cu) commonly called brass have excellent properties such as mechanical strength, malleability and resistance against corrosion; in addition, they are considered to be weakly harmful to the environment[1,2]. On the other hand, molybdenum (Mo) compounds and oxides are also relevant in terms of their excellent resistance against corrosion and electrocatalytic activities[3-10]. Therefore, an alloy/composite composed of Cu, Zn and Mo may have applicability as corrosion resistant coating and electrocatalytic material. Methods that use thermal energy, such as thermal spraying[11] and melting metal in a vacuum or inert atmosphere[12], are utilized to get these materials, but both methods are costly and expend a great deal of energy[13]. A reasonable option is electroplating because it is a generally simple technique, inexpensive and broadly utilized in the production of composites, metallic coatings, alloys and semiconductors on different substrates[14,15].

Recent research shows the possibility of Mo deposition with Zn and Cu[14,16-18]. In these studies, the Zn-Mo composite is proposed as a corrosion resistant coating with low danger and environmentally friendly, in contrast to other anticorrosive alloys containing cadmium and chromium. One of the announced methods for getting this material was by potentiostatic deposition at -1.4 V, where an amount of 70% m/m Mo was incorporated on the surface of the coating[14]. Kazimierczak *et al.*, in another study,

Eclética Química Journal, vol. 44, special issue, 2019, 26-35
ISSN: 1678-4618
DOI: 10.26850/1678-4618eqj.v44.1SI.2019.p26-35

obtained Zn-Mo coatings with up to 14% Mo and showed that the deposits with more than 1% Mo had amorphous or nanocrystalline characteristics[16]. In their turn, Cu-Mo compounds can be used as heat sinks or heat diffusers in electronic devices. Gotou *et al.*[17] studied this system and obtained coatings with up to 22% m/m Mo with amorphous features, regardless of the amount of Mo in the coatings. Thus, a few studies have reported on Cu-Mo and Zn-Mo binary composites; however, there has been no report of Cu-Zn-Mo ternary system obtained by electrodeposition. As previously mentioned, the combination of these three elements could be interesting as a corrosion resistant coating, as with the case of Zn-Cu[19-21] and Zn-Mo[14,16,18] alloys and composites. In addition, the introduction of Mo in these coatings should significantly improve the electrocatalytic properties for water electrolysis because the presence of Mo in the iron group's alloys and composites has been described as responsible for the reduction of the overpotential of the hydrogen evolution reaction[10,22-24].

One of the issues in the electrodeposition of ternary systems is the stability and solubility of the salts used to formulate the deposition baths, which can be achieved by inserting specific complexing agents[25]. However, aggressive and toxic complexes such as cyanides and chlorides are commonly used in the deposition baths of Zn and Cu alloys[26]. In the perspective of environmental problems, it is proposed to utilize a complexing agent that stabilizes the electroactive species and is minimally aggressive and toxic. A complexing agent that fits this proposition is citrate; it is nontoxic and forms electroactive complexes with Cu (II) and Mo (VI) over a wide pH range and with Zn (II) at acidic pH[14,27,28].

Considering these facts, the objective of this study was to propose a bath for electrodeposition of the ternary system with Cu (II), Zn (II) and Mo (VI) ions and to verify the conditions for the occurrence of the co-deposition of these three elements. For this, several molar ratios of the ions in the deposition bath were studied using sodium citrate as complexing agent, and morphological, compositional and crystallographic characterizations of the coatings were performed.

2. Experimental

The chemicals used were $CuSO_4 \cdot 5H_2O$ (> 99%), $ZnSO_4.7H_2O$ (> 99%), Na_2MoO_4 (> 99%) and sodium citrate ($Na_3C_6H_5O_7$ > 99%), all analytical grade and without any purification. The electrolytic baths were prepared by the dissolution of sodium citrate in ultrapure water treated in the Milli-Q system (18.2 MΩ cm^{-1}), followed by the addition of the salts of the metal ions. According to the work of Kazimierczak *et al.*[16] and Slupska and Ozga[29], which correlated the predominant Cu (II), Mo (VI) and Zn (II) species with respect to citrate concentrations and pH in the baths. For that all species to be electroactive in the baths the pH of the electrolyte should be between 3 and 5.5. Therefore, the pH of the electrolytic baths in this work was adjusted to 4 with sulfuric acid. The chemical composition of all baths is shown in Table 1.

Table 1. Chemical composition of the deposition baths used.

Baths	[Mo(VI)]/ mol L^{-1}	[Zn(II)]/ mol L^{-1}	[Cu(II)]/ mol L^{-1}	[Citrate]/ mol L^{-1}	[Mo(VI)]:[Zn(II)]: [Cu(II)]
1	-	0.04	0.02	0.1	0:2:1
2	0.04	-	0.02	0.1	2:0:1
3	0.04	0.04	0.02	0.1	2:2:1
4	0.06	0.04	0.02	0.1	3:2:1
5	0.08	0.04	0.02	0.1	4:2:1

A platinum disk of 0.1 cm^2 was used as the working electrode in the voltammetric studies. It was sanded in 0.25 μm diamond paste and then remained in sonication for 5 min in isopropyl alcohol before being rinsed with deionized water. The coatings were also produced in 1010 carbon steel. For this, steel plates with exposed area of 2.6 cm^2 were used as working electrodes. The plates were treated with 5% sulfuric acid solution to remove the iron oxides. Then, they were rinsed with distilled water and sanded with sandpaper until the granulometry reached 600, and finally

Eclética Química Journal, vol. 44, special issue, 2019, 26-35
ISSN: 1678-4618
DOI: 10.26850/1678-4618eqj.v44.1SI.2019.p26-35

they underwent basic degreasing in NaOH 3.0 mol L^{-1} for 2 min. An $Ag_{(s)}|AgCl_{(s)}|Cl^-$ (saturated KCl) electrode and a high surface area Pt grid were used as reference and auxiliary electrodes, respectively.

The voltammetric studies were performed in the potentials range of 1.5 to -1.5 V with a scan rate of 50 mV s^{-1}, three cycles were performed in each measurement. The deposition potentials were evaluated through cyclic voltammetry at different cathodic inversion potentials in the range of -1.0 to -2.0 V with a scan velocity of 50 mV s^{-1}. Electrochemical stripping analyses in the range of -1.0 to 1.0 V were obtained for the coatings deposited in -1.6, 1.75 and -2.0 V in the binary baths of Mo (VI) and Cu (II) (bath 4) and Zn (II) and Cu (II) (bath 5). The stripping analyses were carried out in 0.1 mol L^{-1} sodium citrate solution at pH 4. The depositions were performed at constant potential in the range of -1.2 to -2.0 V for 1800 s. All measurements were performed at 25° C. The morphologies of the coatings were evaluated using scanning electron microscopy (SEM) with high-resolution field emission using an FE-SEM, ZEISS SUPRA 35, and the composition was analyzed through X-ray dispersive energy (EDX) spectroscopy using a FEI-XL30-FEG with an Oxford Instruments-Link ISIS 300 detector. The structural characterizations were performed using an X-ray diffractometer (Rigaku-DMax2500PC) with Cu Kα = 1.5406Å, 40 kV voltage, theta-2theta configuration and a scan angle of 20-80º with a scanning speed of 2°/min.

3. Results and discussion

3.1. Voltammetric studies

The cathodic voltammograms for the baths with 2:2:1, 3:2:1 and 4:2:1 molar ratios of Mo(VI): Zn(II): Cu(II) on Pt are shown in Fig. 1. The peak c1 at 0.15 V and c2 at -0.1 V could be attributed to underpotential deposition (UPD) and bulk deposition of copper from the non-complexed Cu^{2+} ions, respectively[30]. This is possible because the concentration of citrate (0.1 mol L^{-1}) in these baths was less than the total metal-ion concentration, which is evidence of the occurrence of Mo (VI), Zn (II) and Cu (II) noncomplexed species. It was also observed that peaks c1 and c2 presented higher cathodic currents when the concentration of molybdate was increased in the baths. Since the molybdenum(VI) citrate complexes are more stable that copper (II) citrate complexes in the pH used, the increase of the concentration of MoO_4^{2-} ions led to a higher concentration of free Cu^{2+} ions in the bath[31,32]. The increase of the Mo (VI) concentration caused a considerable increase in the peak current c3 in the region of -0.8 V, which was attributed to the deposition of molybdenum oxides/hydroxides (Fig. S1b). The peaks c4 and c5 were due to the reduction of Cu (II) and Zn (II) complexed with citrate, respectively (Fig. S1). The curves in Fig. 1 indicate that the cathodic current in potentials more negative than -1.25 V increased more significantly in the bath with a higher concentration of MoO_4^{2-} (curve 3). This current is due to the evolution of H_2, which is facilitated by the higher amount of Mo oxides/hydroxides deposited that is a catalytic species for hydrogen evolution reaction (HER)[33]. In conclusion, an increase of MoO_4^{2-} concentration in the baths facilitates the deposition of molybdenum species; however, it leads to a higher evolution of hydrogen, which can lead to lower deposition efficiency and poor structure of the coatings.

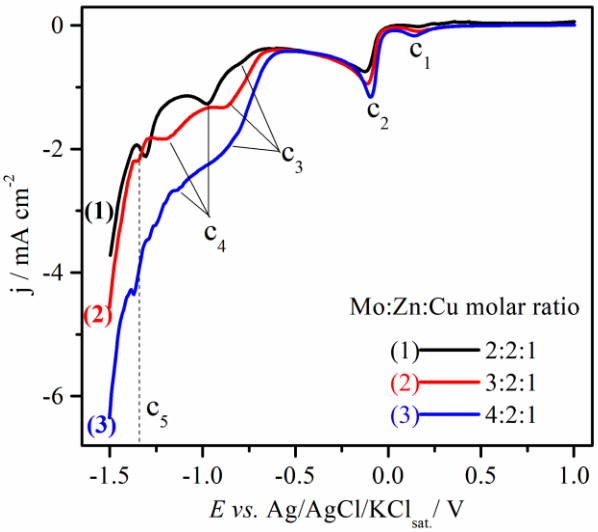

Figure 1. Cathodic voltammograms on Pt for baths Mo: Zn: Cu of molar ratios (1) 2: 2: 1 (bath 6), (2) 3: 2: 1 (bath 7) and 4: 2: 1 (bath 8) at T = 25 °C.

To find the best cathodic deposition potentials, a study was performed on different inversion cathodic potentials in the 2:2:1 Mo: Zn: Cu bath (bath 6), as shown in Fig. 2a. From -1.3 V, the currents were very high due to the HER (graph inserted in Fig. 2a), which made it difficult to visualize the processes; therefore, the study focused on the more positive potential regions.

ISSN: 1678-4618
DOI: 10.26850/1678-4618eqj.v44.1SI.2019.p26-35

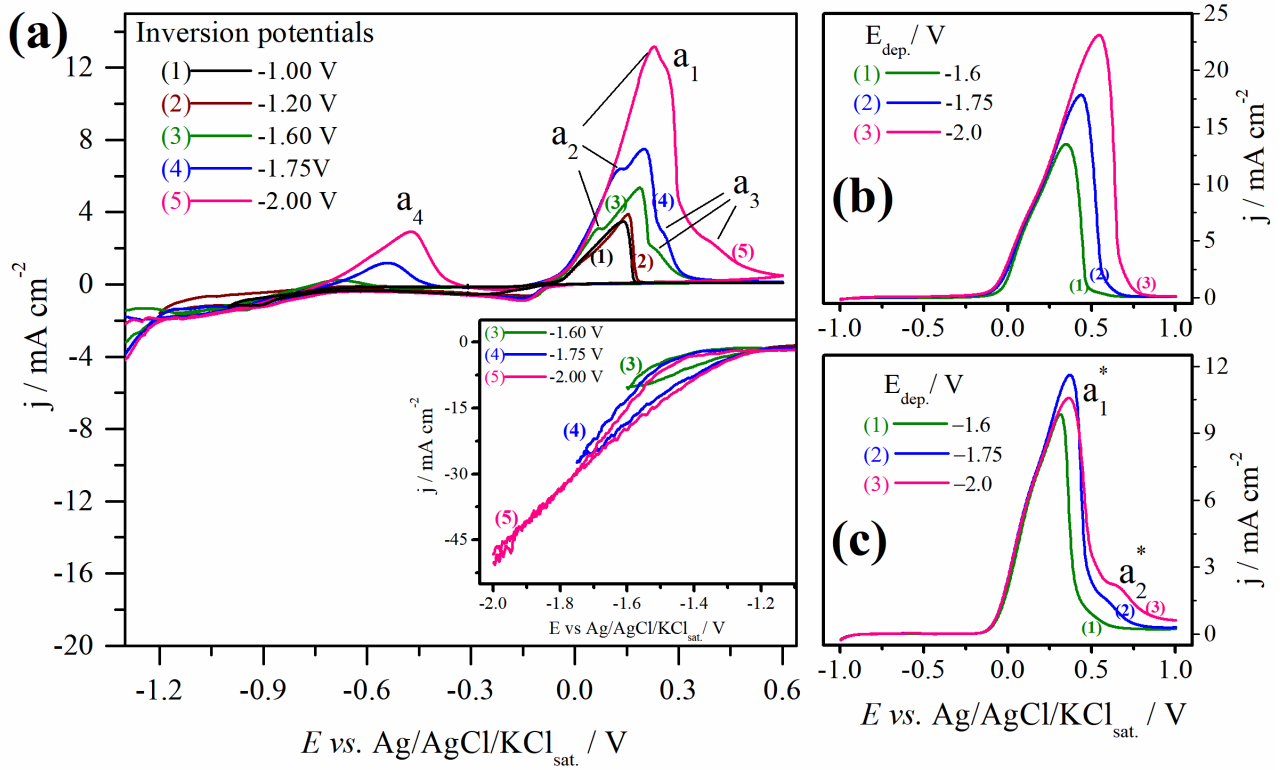

Figure 2. (a) Voltammograms on Pt for bath 3 of 2:2:1 molar ratio of Mo: Zn: Cu at inversion potentials -1.0V (line 1), -1.2 V (line 2), -1.6 (line 3), -1.75 V (line 4) and -2.0 V (line 5). (b) Stripping voltammetry curves for the coatings obtained on Pt in the bath 1 at -1.6, -1.75 and -2.0 V (b) stripping voltammetry curves for the coatings obtained on Pt in the bath 2 at -1.6, -1.75 and -2.0 V at T = 25 °C.

In the inversion potentials at -1.0 (line 1) and -1.2 V (line 2), only a cathodic and an anodic peak in the range of potentials of -0.25 to 0.25 V were identified as being attributed to deposition and dissolution of Cu. From the potential of inversion of -1.6 V, a peak (a2) attributed to the dissolution of zinc or zinc-rich phase appeared, and for the more negative potentials (-1.75 and -2.0 V), larger anodic currents were presented, showing the favoring of the deposition of zinc at more negative potentials. The oxidation peaks in the range of 0 to 0.52 V potentials (a1, a2 and a3) that appeared for the inverse potentials -1.6 (line 3), -1.75 (line 4) and -2.0 V (line 5) are attributed to the dissolution of copper and copper-rich phases. It can be concluded from the voltammetric studies that zinc-rich Cu-Zn phases and Cu-Mo composites can be electrodeposited at highly negative potentials simultaneously with the HER from the proposed baths.

The phases related to the anode peaks in the region of potentials of 0.0 to 0.52 V (a1, a2 and a3) cannot be identified only by the voltammograms in Fig. 2a. Therefore, electrochemical stripping analyses were performed for deposits obtained in the Zn(II): Cu(II) (bath 4) and Mo(VI): Cu(II) (bath 5) binary baths. The coatings were deposited in -1.6, -1.75 and -2.0 V for 5 min on Pt; these curves are shown in Fig. 2b and c, respectively. The stripping curves for the coatings obtained in the bath containing only Zn (II) and Cu (II) presented a shoulder followed by a peak with high anodic current, which was attributed to the dissolution of Cu and Cu-Zn phases. This result enables affirmation that peaks a1 and a2 observed in the voltammograms of Fig. 2a were due to the dissolution of Cu-Zn phases formed in potentials more negative than -1.2 V. The attribution of this anodic process to the dissolution of the Cu-Zn is coherent because this process occurs in more negative potentials in comparison to the potential dissolution of the Cu, motivated by the presence of Zn atoms.

Figure 2b shows the stripping curves for the coatings obtained in the bath containing only Mo (VI) and Cu (II). In this voltammogram, one shoulder can be observed followed by the a1* peak attributed to the dissolution of Cu and a2* peak

Eclética Química Journal, vol. 44, special issue, 2019, 26-35
ISSN: 1678-4618
DOI: 10.26850/1678-4618eqj.v44.1SI.2019.p26-35

shifted to more positive potentials attributed to the phase dissolution or intermetallic compound formed between Cu and Mo. The shift of the a2* peak to more positive potentials compared to the oxidation of Cu is coherent because Mo has passivating characteristics. In turn, this result indicates that the anodic process a3 in the voltammograms of Fig. 2a is due to dissolution of Cu-Mo phases. The stripping curves confirm the assumption that Cu, Mo and Zn containing intermetallic compounds can be formed from that bath at potentials more negative than the Zn reduction potential, together with HER.

3.2. Physical characterization

Aiming for future applications, the coatings were also produced in 1010 carbon steel and characterized by their morphologies, chemical compositions and crystalline structure. The amount of the Mo, Cu and Zn in the coatings obtained at -1.5 V on 1010 steel in the 2:2:1, 3:2:1 and 4:2:1 molar ratios of Mo: Zn: Cu are shown in Fig. 3. The amount of Cu was the largest of the three metals in the system, varying between 30 and 40% at/at, showing that copper is deposited preferentially in this deposition conditions. However, the increased deposition of Mo-oxidized species with increasing MoO_4^{2-} concentration in the baths directly affected Cu deposition by reducing its content in the coatings. Large amounts of Zn were also deposited, and all coatings that exhibited 20 to 28% of these metal coatings had less than 10% of Mo; on the other hand, they had considerable amounts of oxygen (more than 30% at). From Fig. 3, it is clear that an increase of the Mo content in coatings leads to an increase in the oxygen content, which is independent of the Cu or Zn, indicating that the Mo in the coatings is in the form of oxides. To understand the influence of the deposition potential on the coatings' chemical composition, electrodepositions were performed in a potential range of -1.2 to -1.9 V in the 4:2:1 molar ratio (bath 5) on steel 1010. These data are presented in Fig. 4a without the oxygen contents. It is noticed that the higher Mo contents were deposited at potentials more positive than -1.4 V. However, in comparison to the Cu and Zn contents, the amount of Mo remained almost constant in all deposition potentials, showing that the applied overpotential has little influence on its electrodeposition. On the other hand, both Cu and Zn deposition are strongly dependent on the overpotential applied. At the potentials more positive than -1.4 V the coatings consisted of approximately 70 to 75% of Cu and between 13 and 15% of Zn, but in more negative potentials, the Zn deposition was favored, becoming the major component with approximately 54% in -1.9 V. Based in Fig. 1, it is possible to infer that copper deposition occurs via kinetically activated regime until the potential near -1.2 V, followed by a diffusion process at more negative potentials. It is agreement the fact that a smaller amount of copper was electrodeposited in more negative potentials. On the other hand, the electrodeposition of zinc was favored in potentials more negative than -1.2 V due this process is activated kinetically. This shows that, depending on the excess potential applied, it is possible to obtain coatings with different compositions. For more positive potentials, Cu rich coatings and for more negative potentials, Zn rich coatings are obtained.

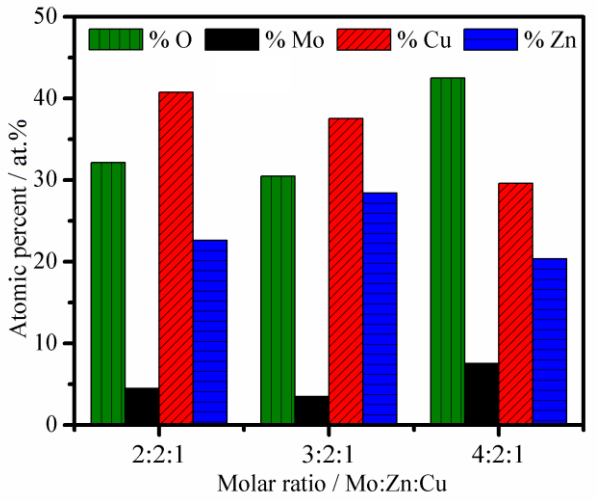

Figure 3. Composition for the coatings obtained in the baths of 2:2:1 (bath 3), 3:2:1 (bath 4) and 4:2:1 (bath 5) molar ratio of Mo: Zn: Cu at -1.5 V on 1010 steel substrate.

Eclética Química Journal, vol. 44, special issue, 2019, 26-35
ISSN: 1678-4618
DOI: 10.26850/1678-4618eqj.v44.1SI.2019.p26-35

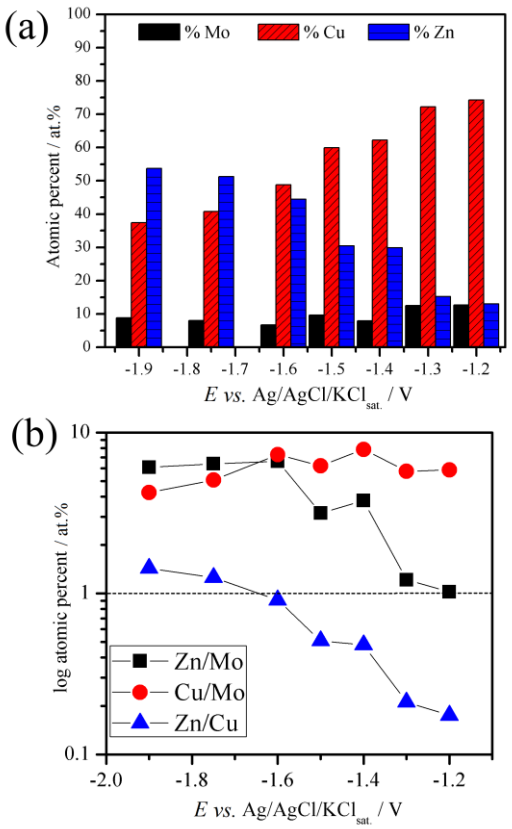

Figure 4. (a) Composition for the coatings obtained in the bath 5 of molar ratio Mo: Zn: Cu 4:2:1 in the range of deposition potentials of -1.2 to -1.9 V. (b) molar ratio between the metals in the coatings obtained in the bath 5 in the range of deposition potentials of -1.2 to -1.9 V on 1010 steel substrate.

The profiles of the atomic ratios between the metals in the coatings are shown in Fig. 4b. Comparing the profiles of the Zn/Cu and Zn/Mo atomic ratios indicates that in the coatings obtained over the entire range of deposition potentials, the ratio values grew following the same pattern. The values of the Zn/Cu ratio in the most positive potentials were less than 1.0 (higher Cu content) and remained thus until the potential of -1.6 V, where the Cu and Zn contents were similar. In the most negative potentials, Zn electrodeposition was favored, and the Zn/Cu ratio values were greater than 1.0 (higher Zn content). The profile observed for the Zn/Mo ratio was similar to that observed in Zn/Cu, indicating that the behavior of Mo and Cu deposition in relation to Zn deposition is similar; that is, in more positive potentials, Cu and Mo deposition is favored, and a smaller amount of Zn is deposited. According to the Cu/Mo ratio profile, there was a small dependence between Cu and Mo on their deposition, as evidenced by the smaller variation of these values in comparison with the Zn/Mo and Zn/Cu ratios.

The coating surface morphologies obtained in the -1.5 V potential are shown in Fig. 5a. They presented a relatively compact structure with small agglomerated particles forming larger cauliflower-like structures; the small, smooth agglomerates on these structures are attributed to the oxides of Mo. The coating obtained in the 3:2:1 bath (Fig. 5b) showed structures similar to that of the 2:2:1 film but with a greater number of smooth structures between and on the grains. In contrast, the coating obtained in the 4:2:1 bath (Fig. 5c) presented less compactness and uniformity in its structure. The variation of the coating obtained in the bath with the higher concentration of Mo can be explained by taking into account the greater evolution of hydrogen that occurs with the electrodeposition of the coatings. This meant that the growth on the substrate was not uniform and compact. The greatest hydrogen evolution from bath 5 is proven by the cathodic voltammetry shown in Fig. 1, in which the cathodic current at -1.5 V related to HER for this bath was considerably higher compared to the currents obtained in the other baths at the same potential.

ISSN: 1678-4618
DOI: 10.26850/1678-4618eqj.v44.1SI.2019.p26-35

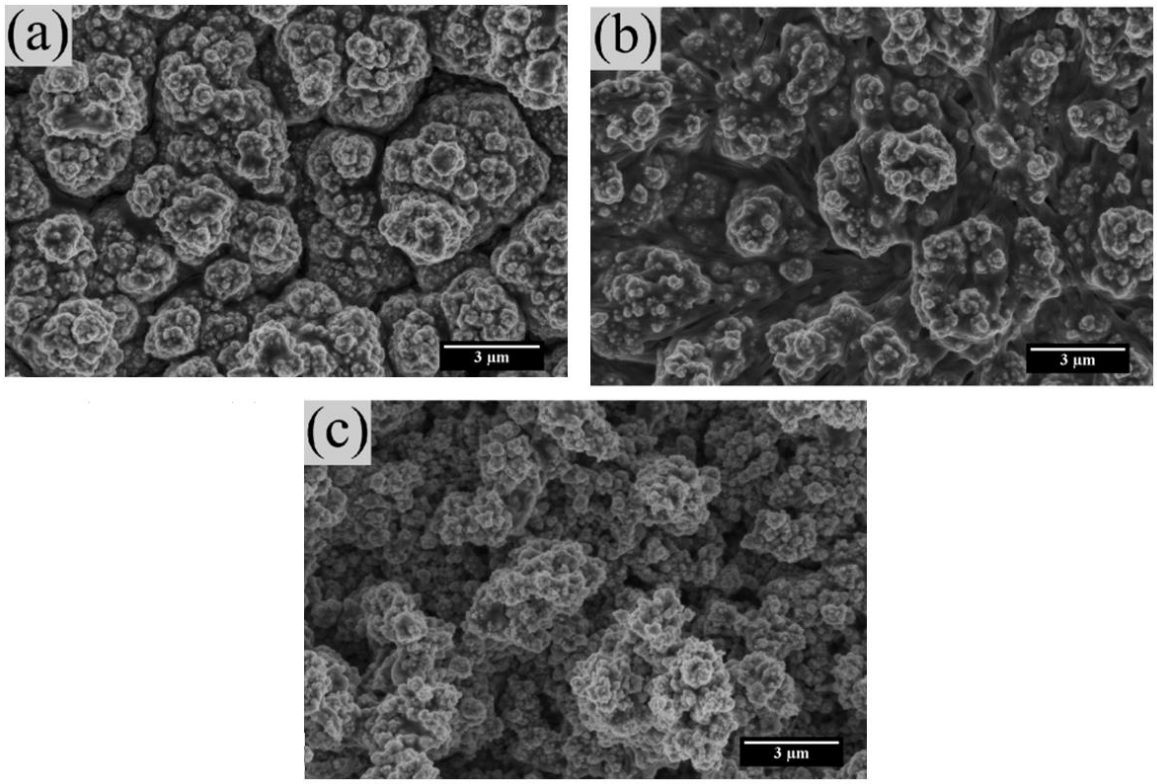

Figure 5. Surface morphologies obtained by SEM for coatings obtained at -1.5 V in baths with Mo: Zn: Cu molar ratio of (a) 2:2:1 (bath 3), (b) 3:2:1 (bath 4) and (c) 4:2:1 (bath 5) on 1010 steel substrate.

The crystal structures were evaluated using X-ray diffraction (XRD) and are shown in Fig. 6. The phases were identified with the aid of the crystallographic data patterns.

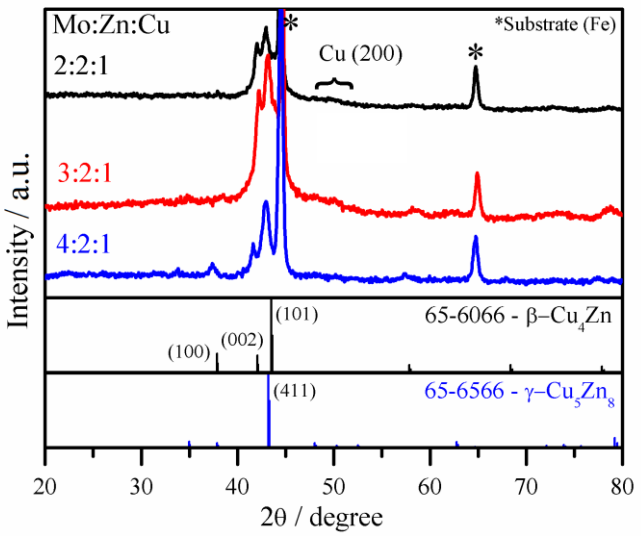

Figure 6. X-ray diffraction patterns for coatings obtained at -1.5 V in baths of Mo: Zn: Cu molar ratios of 2:2:1 (bath 3, black line), 3:2:1 (bath 4, red line) and 4:2:1 (bath 5, blue line) on 1010 steel substrate.

For all coatings, two phases of the Cu-Zn alloy were identified, β-Cu-Zn (PDF # 65-6066) and γ-Cu-Zn (PDF # 65-6566). The equilibrium phase diagram for Cu-Zn alloys shows that Cu-rich phases, such as α-Cu-Zn (99-70% Cu) and β-Cu-Zn (with up to 48% Zn), and Zn-rich phases, such as γ-Cu-Zn (Cu_5Zn_8, with up to 66% Zn) and ε-Cu-Zn_5, are possible to obtain through electrodeposition[21].

The identified β-Cu-Zn and γ-Cu-Zn phases are consistent with composition data shown in Fig. 3, where all coatings contained 30 to 50% Cu and 25 to 35% Zn. However, no peaks of Mo or oxidized species of this metal were observed, although these coatings had up to 8% of Mo, indicating that the electrodeposited Mo species are totally amorphous. On the other hand, diffraction patterns showed significant irregularity in background intensity, most evident in the range of 2θ from 50º to 53º. This irregularity was attributed to the diffraction of plane (200) of the Cu with low crystallinity, which might have been caused by the introduction of amorphous Mo into the lattice of this metal. According to Gotou *et al.*[17], molybdenum can be introduced into the crystal lattice of the copper, causing an enlarging of lattice space and leading to

Eclética Química Journal, vol. 44, special issue, 2019, 26-35
ISSN: 1678-4618
DOI: 10.26850/1678-4618eqj.v44.1SI.2019.p26-35

an amorphous structure. Therefore, the Cu-Zn-Mo coatings obtained in this work were a mixture of Cu-Zn intermetallic phases and copper-molybdenum amorphous composites, as well as Mo oxides with fully amorphous characteristics.

4. Conclusions

In this work was studied the parameters for electrodeposition of the system Cu-Zn-Mo in citrate baths. The voltammetric profiles indicate that binary phases of Cu-Zn and Cu-Mo can be formed in potentials more negative than -1.2 V together with hydrogen evolution. The morphologies of the coatings obtained in the potential of -1.5 V were compact and presented small agglomerated particles forming larger cauliflower structures, and Mo, Cu and Zn in these coatings ranged from 5 to 8%, 30 to 40% and 20 to 28%, respectively. Compositional analysis and XRD patterns showed that no ternary phases were formed, but rather a mixture of intermetallic Zn-Cu phases and Mo-Cu amorphous composite, as well as Mo oxides with totally amorphous characteristics.

5. Acknowledgments

The authors thank the Conselho Nacional de Desenvolvimento Científico e Tecnológico (CNPq), Fundação de Amparo à Pesquisa do Estado de São Paulo (FAPESP number 2018/16401-8), CEPID (2013/07296-2) and CAPES (finance code 001) for financial support.

See **Supplementary information**.

6. References

[1] Morales, J., Fernandez, G. T., Esparza, P., Gonzalez, S., Salvarezza, R. C., Arvia, A. J., A comparative study on the passivation and localized corrosion of α, β, and α+β brass in borate buffer solutions containing sodium chloride-I. Electrochemical data, Corrosion Science 37 (2) (1995) 211-229. https://doi.org/10.1016/0010-938X(94)00108-I.

[2] Lowenheim, F. A., Modern Electroplating, Wiley-Interscience, New York, 3rd ed., 1974.

[3] Gómez, E., Pellicer, E., Vallés, E., Influence of the bath composition and the pH on the induced cobalt-molybdenum electrodeposition, Journal of Electroanalytical Chemistry 556 (2003) 137-145. https://doi.org/10.1016/S0022-0728(03)00339-5.

[4] Sanches, L. S., Domingues, S. H., Carubelli, A., Mascaro, L. H., Electrodeposition of Ni-Mo and Fe-Mo alloys from sulfate-citrate acid solutions, Journal of Brazilian Chemical Society 14 (4) (2003) 556-563. https://doi.org/10.1590/S0103-50532003000400011.

[5] Sanches, L. S., Domingues, S. H., Marino, C. E. B., Mascaro, L. H., Characterisation of electrochemically deposited Ni-Mo alloy coatings, Electrochemistry communication 6 (6) (2004) 543-548. https://doi.org/10.1016/j.elecom.2004.04.002.

[6] Podlaha, E. J., Landolt, D., Induced codeposition: II. A mathematical model describing the electrodeposition of Ni-Mo alloys, Journal of The Electrochemical Society. 143 (3) (1996) 893-899. https://doi.org/10.1149/1.1836553.

[7] Gómez, E., Pellicer, E., Duch, M., Esteve, J., Vallés, E., Molybdenum alloy electrodeposits for magnetic actuation, Electrochimica Acta 51 (16) (2006) 3214-3222. https://doi.org/10.1016/j.electacta.2005.09.010.

[8] Saravanan, P., Raja, V. S., Mukherjee, S., Effect of alloyed molybdenum on corrosion behavior of plasma immersion nitrogen ion implanted austenitic stainless steel, Corrosion Science 74 (2013) 106-115. https://doi.org/10.1016/j.corsci.2013.04.030.

[9] Liu, R., Yao, J., Zhang, Q., Yao, M. X., Collier, R., Effects of molybdenum content on the wear/erosion and corrosion performance of low-carbon Stellite alloys, Materials & Design 78 (2015) 95-106. https://doi.org/10.1016/j.matdes.2015.04.030.

[10] Xia, M., Lei, T., Lv, N., Li, N., Synthesis and electrocatalytic hydrogen evolution performance of Ni-Mo-Cu alloy coating electrode, International Journal of Hydrogen Energy 39 (10) (2014) 4797-4802. https://doi.org/10.1016/j.ijhydene.2014.01.091.

[11] Babu, M. V, Kumar, R. K., Prabhakar, O., Shankar, N. G., Simultaneous optimization of flame spraying process parameters for high quality molybdenum coatings using Taguchi methods, Surface and Coatings Technology 79 (1-3) (1996) 276-288. https://doi.org/10.1016/0257-8972(95)02453-0.

[12] Savitskii, E. M., Burkhanov, G. S., Physical metallurgy of refractory metals and alloys, Consultants Bureau, New York, 1st ed., 1970.

[13] Syed, R., Ghosh, S. K., Sastry, P. U., Sharma, G., Hubli, R. C., Chakravartty, J. K., Electrodeposition of thick metallic amorphous molybdenum coating from aqueous electrolyte, Surface Coatings Technology 261

ISSN: 1678-4618
DOI: 10.26850/1678-4618eqj.v44.1SI.2019.p26-35

(2015) 15-20. https://doi.org/10.1016/j.surfcoat.2014.11.073.

[14] Kazimierczak, H., Ozga, P., Socha, R. P., Investigation of electrochemical co-deposition of zinc and molybdenum from citrate solutions, Electrochimica Acta 104 (2013) 378-390. https://doi.org/10.1016/j.electacta.2012.12.140.

[15] Gromboni, M. F., Mascaro, L. H., Optical and structural study of electrodeposited zinc selenide thin fi lms, Journal of Electroanalytical Chemistry 780 (2016) 360-366. https://doi.org/10.1016/j.jelechem.2016.04.037.

[16] Kazimierczak, H., Ozga, P., Swiatek, Z., Bielanska, E., Characterisation of Zn-Mo alloy layers electrodeposited from aqueous citrate solution, Journal of Alloys and Compounds 578 (2013) 82-89. https://doi.org/10.1016/j.jallcom.2013.04.205.

[17] Gotou, M., Arakawa, T., Watanabe, N., Hara, T., Tomita, T., Hashimoto, A., Takanashi, H., Koiwa, I., Copper-molybdenum source ratio and complexing agent for high molybdenum content in electrodeposited Cu-Mo, Journal of The Electrochemical Society 161 (12) (2014) D628-D631. https://doi.org/10.1149/2.0051412jes.

[18] Kazimierczak, H., Ozga, P., Berent, K., Kot, M., Microstructure and micromechanical properties of electrodeposited Zn-Mo coatings on steel, Journal of Alloys and Compounds 636 (2015) 156-164. https://doi.org/10.1016/j.jallcom.2015.02.165.

[19] de Almeida, M. R. H., Barbano, E. P., Zacarin, M. G., Brito, M. M., Tulio, P. C., Carlos, I. A., Electrodeposition of CuZn films from free-of-cyanide alkaline baths containing EDTA as complexing agent, Surface and Coatings Technology 287 (2016) 103-112. https://doi.org/10.1016/j.surfcoat.2015.12.079.

[20] Özdemir, R., Karahan, İ. H., Karabulut, O., A study on the electrodeposited Cu-Zn alloy thin films, Metallurgical and Materials Transactions A 47 (11) (2016) 5609-5617. https://doi.org/10.1007/s11661-016-3715-0.

[21] Juskenas, R., Karpaviciene, V., Pakstas, V., Selskis, A., Kapocius, V., Electrochemical and XRD studies of Cu-Zn coatings electrodeposited in solution with d-mannitol, Journal of Electroanalytical Chemistry 602 (2) (2007) 237-244. https://doi.org/10.1016/j.jelechem.2007.01.004.

[22] Wang, X., Su, R., Aslan, H., Kibsgaard, J., Wendt, S., Meng, L., Dong, M., Huang, Y., Besenbacher, F., Tweaking the composition of NiMoZn alloy electrocatalyst for enhanced hydrogen evolution reaction performance, Nano Energy 12 (2015) 9-18. https://doi.org/10.1016/j.nanoen.2014.12.007.

[23] Luo, D., Hu, W., Wang, Y., Zhang, Y., Wang, G., Study on amorphous Ni-Mo-Fe-Zn coating electrocatalyst for hydrogen evolution in alkaline solution, Journal of Mechanical Science and Technology 12 (3) (1996) 190-194.

[24] Arul Raj, I., On the catalytic activity of NiMoFe composite surface coatings for the hydrogen cathodes in the industrial electrochemical production of hydrogen, Applied Surface Science 59 (3-4) (1992) 245-252. https://doi.org/10.1016/0169-4332(92)90124-G.

[25] Gamburg, Y. D., Zangari, G., Theory and Practice of Metal Electrodeposition, Springer, New York. 1st ed., 2011.

[26] Loto, C. A., Electrodeposition of zinc from acid based solutions: A review and experimental study, Asian Journal Applied Sience 5 (6) (2012) 314-326. https://doi.org/10.3923/ajaps.2012.314.326.

[27] Beltowska-Lehman, E., Electrodeposition of protective Ni-Cu-Mo coatings from complex citrate solutions, Surface Coatings Technology 151-152 (2002) 440-443. https://doi.org/10.1016/S0257-8972(01)01613-9.

[28] Silva, F. L. G., Do Lago, D. C. B., D'Elia, E., Senna, L. F., Electrodeposition of Cu-Zn alloy coatings from citrate baths containing benzotriazole and cysteine as additives, Journal of Applied Electrochemistry 40 (11) (2010) 2013-2022. https://doi.org/10.1007/s10800-010-0181-z.

[29] Slupska, M., Ozga, P., Electrodeposition of Sn-Zn-Cu alloys from citrate solutions, Electrochimica Acta 141 (2014) 149-160. https://doi.org/10.1016/j.electacta.2014.07.039.

[30] Alonso, C., Pascual, M. J., Abruña, H. D., Influence of organic adsorbates on the under and overpotential deposition of copper on polycrystalline platinum electrodes, Electrochimica Acta 42 (11) (1997) 1739-1750. https://doi.org/10.1016/S0013-4686(96)00374-X.

[31] Cruywagen, J. J., Rohwer, E. A., Wessels, G. F. S., Molybdenum(VI) complex formation-8. Equilibria and thermodynamic quantities for the reactions with citrate, Polyhedron 14 (23-24) (1995) 3481-3493. https://doi.org/10.1016/0277-5387(95)00210-J.

[32] Field, T. B., McCourt, J. L., McBryde, W. A. E., Composition and stability of iron and copper citrate complexes in aqueous solution, Canadian Journal of Chemistry 52 (17) (1974) 3119-3124. https://doi.org/10.1139/v74-458.

ISSN: 1678-4618
DOI: 10.26850/1678-4618eqj.v44.1SI.2019.p26-35

[33] Luo, Z., Miao, R., Huan, T. D., Mosa, I. M., Poyraz, A. S., Zhong, W., Cloud, J. E., Kriz, D. A., Thanneeru, S., He, J., Zhang, Y., Ramprasad, R., Suib, S. L., Mesoporous MoO-x material as an efficient electrocatalyst for hydrogen evolution reactions, Advanced Energy Materials 6 (16) (2016) 1600528. https://doi.org/10.1002/aenm.201600528.

ISSN: 1678-4618
DOI: 10.26850/1678-4618eqj.v44.1SI.2019.p26-35

Eclética Química Journal

Supplementary Information
iq.unesp.br/ecletica

| Vol. 44 | special issue | 2019 |

Supplementary Information

Electrodeposition study of the Cu-Zn-Mo system in citrate/sulfate medium

Hugo Sousa Santos[1], Alessandra Alves Correa[1], Murilo Fernando Gromboni[2], Lucia Helena Mascaro[1+]

1.Federal University of São Carlos (UFSCar), Department of Chemistry, Km 235 Washington Luís Hw, São Carlos, São Paulo, Brazil
2.University of São Paulo (USP), Institute of Chemistry, 400 Trabalhador São Carlense Ave, São Carlos, São Paulo, Brazil

[+]Corresponding author: Lucia Helena Mascaro, phone: +55 16 33519698, email address: lmascaro@ufscar.br

ARTICLE INFO

Article history:
Received: January 16, 2019
Accepted: August 3, 2019
Published: November 20, 2019

Keywords:
1. electrodeposition
2. Cu-Zn-Mo system
3. composite
4. alloy
5. intermetallic phases
6. molybdenum oxides

The electrochemical behavior of the individual ions (Mo (VI), Zn (II) and Cu (II)) as well as for the ternary bath in the 2:2:1 molar ratio of Mo:Zn:Cu (bath 3) on Pt was studied by cyclic voltammetry and are shown in Fig. S1.

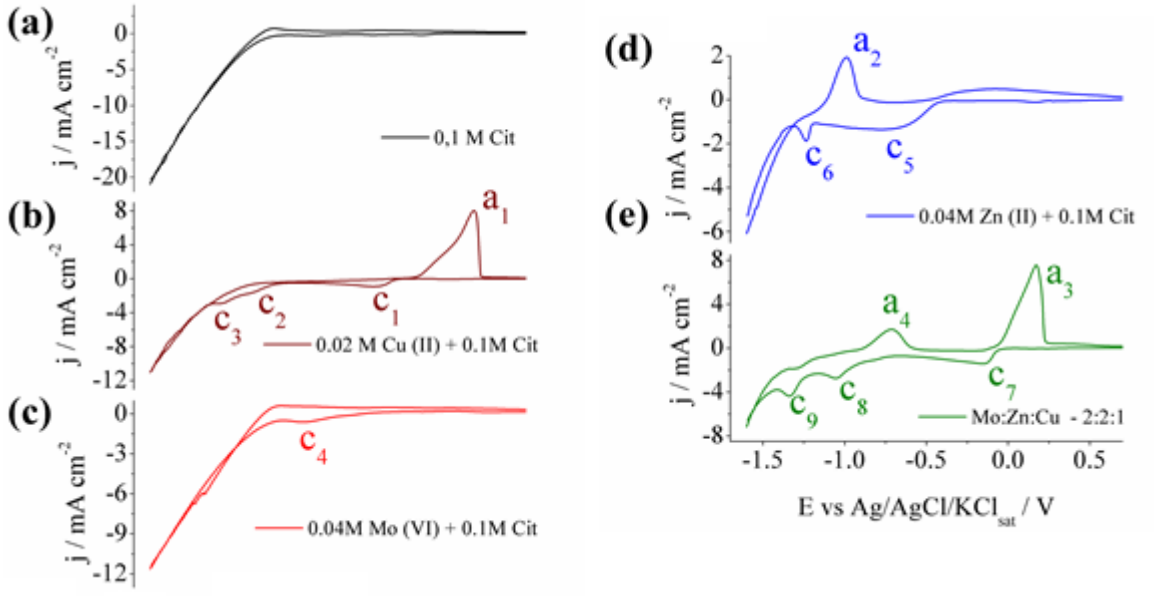

Figure S1. Cyclic voltammograms obtained on Pt in (a) 0.1 mol L^{-1} of sodium citrate, (b) 20 mmol L^{-1} of $CuSO_4$, (c) 40 mmol L^{-1} of Na_2MoO_4, (d) 40 mmol L^{-1} of $ZnSO_4$ and 0.1 mol L^{-1} of citrate and (e) 2:2:1 molar ratio bath (40 Mo (VI) + 40 Zn (II) + 20 Cu (II) mmol L^{-1}).

The voltammogram of a solution without the metal ions (Cu (II), Zn (II) and Mo (VI), only with sodium citrate, is shown in Fig. 1Sa. The voltammogram shows no clear anode and cathode

Eclética Química Journal, vol. 44, special issue, 2019, 36-38
ISSN: 1678-4618
DOI: 10.26850/1678-4618eqj.v44.1SI.2019.p36-38

peaks, only a high cathodic current in potentials after -1.0 V due to the hydrogen evolution reaction (HER).

In the voltammogram obtained for Cu (II) bath (Fig. S1b) the cathodic processes (c1, c2, and c3) in approximately -0.22, -0.96 and -1.15 V were attributed to the reduction of Cu (II) from different complexes formed between copper and citrate. At the concentration of citrate and pH used, the $[CuH_2Cit]^-$ and $[Cu_2HCit_2]^{3-}$ complexes are the predominant species, with low free Cu^{2+} ions. In the anodic branch, there is a shoulder followed by a peak (a1) in the region of potentials of 0.15 to 0.4 V both attributed to the dissolution of metallic copper deposited in the cathodic sweep[1].

In the voltammogram for Mo (VI) in citrate (Fig. S1c), two cathode processes can be noted, one in the region of -0.6 V (c4) and another in -1.27 V. As metallic molybdenum can't be electrodeposited in solutions of its salts, only in the presence of certain metal ions that induce its co-deposition[2-4], the process c4 is characteristic of the deposition of oxides/hydroxides of Mo. At the concentration of citrate and pH close to those used in this work, the Mo (VI) species are predominantly in the complexed form $[MoO_4H_4Cit]^{2-}$, and the proposed reaction for the formation of Mo oxides from this species is shown in the Eq. S1[5] The small peak at -1.27 V was attributed to the evolution of hydrogen in profusion. During the anodic scan, no process is observed, this phenomenon is attributed to the passivating characteristics of the deposited molybdenum oxides.

$$MoO_4Cit^{3-}_{(aq)} + 3H^+_{(aq)} + 2e^- \rightarrow MoO_{2(s)} + 2H_2O + HCit^{2-}_{(aq)} \quad (1)$$

The cathodic sweep in the voltammogram for Zn (II) in citrate (Fig. S1d) shows a current plateau starting at -0.45 V (c5) and a peak at -1.25 V (c6). In the presence of citrate at pH 4.0 the $ZnHCit^-$ complex is the major species and the processes c5 and c6 corresponding to the reduction of Zn (II) from this complex and the bare Zn^{2+} ions, respectively[1]. In the anodic sweep, only a peak at -1.0 V attributed to the dissolution of electrodeposited Zn is observed.

Figure S1 shows the voltammogram obtained for the bath containing Mo(VI):Zn(II):Cu (II) in the 2:2:1 molar ratio (bath 5). The cathode peak at -0.15 V (c7) can be attributed to the deposition of Cu-rich species because it is in the same potential region of the c1 peak. In the cathodic sweep, two other peaks appear at -1.0 V (c8) and -1.3 V (c9), which compared to Fig. S1b and d, were attributed to Cu (II) reduction from the complexes formed between Cu (II) and citrate and the reduction of Zn (II), respectively. As for the reduction of Mo (VI), does not appear any definite peak in the presence of the three ions, however, a slight shoulder between the c7 and c8 peaks can be observed that is attributed the deposition of oxides/hydroxides of molybdenum. In the anodic scanning the peak of 0.16 V (a3) is attributed to the intermetallic phase oxidation containing in a higher proportion Cu with the other metals (Zn and Mo), since this process when compared to that of the voltammogram containing only Cu ions) (Fig. S1b) is shifted to more negative potentials. On the other hand, the anodic peak (a4) at -0.71 V was attributed to the dissolution of Zn-Cu intermetallic phases rich in Zn, since it appears close to the zinc oxidation region displaced to more positive potentials when compared to the Zn (II) oxidation peak only in citrate (Fig. S1d).

References

[1] Shin, S., Park, C., Kim, C., Kim, Y., Park, S., Lee, J. H., Cyclic voltammetry studies of copper, tin and zinc electrodeposition in a citrate complex system for CZTS solar cell application, Current Applied Physics 16 (2) (2016) 207-210. https://doi.org/10.1016/j.cap.2015.11.017.

[2] Zeng, Y., Li, Z., Ma, M., Zhou, S., In situ surface Raman study of the induced codeposition mechanism of Ni-Mo alloys, Electrochemistry Communications 2 (1) (2000) 36-38. https://doi.org/10.1016/S1388-2481(99)00137-X.

[3] Marlot, A., Kern, P., Landolt, D., Pulse plating of Ni-Mo alloys from Ni-rich electrolytes, Electrochimica Acta 48 (1) (2002) 29-36. https://doi.org/10.1016/S0013-4686(02)00544-3.

[4] Beltowska-Lehman, E., Ozga, P., Chassaing, E., Pulse electrodeposition of Ni-Cu-Mo alloys, Surface and Coatings Technology 78 (1-3) (1996) 233-237. https://doi.org/10.1016/0257-8972(94)02406-5.

ISSN: 1678-4618
DOI: 10.26850/1678-4618eqj.v44.1SI.2019.p36-38

[5] Kazimierczak, H., Ozga, P., Socha, R. P., Investigation of electrochemical co-deposition of zinc and molybdenum from citrate solutions, Electrochimica Acta 104 (2013) 378-390. https://doi.org/10.1016/j.electacta.2012.12.140.

ISSN: 1678-4618
DOI: 10.26850/1678-4618eqj.v44.1SI.2019.p36-38

Eclética Química Journal

Original article
iq.unesp.br/ecletica

| Vol. 44 | special issue | 2019 |

Application of ultrafiltration and electrodialysis techniques in lactic acid removal from whey solutions

Renata Oberherr, Renata Fioravante Tassinary, Letícia Vognach, Simone Stülp+

University of Vale do Taquari (Univates), Center of Sciences and Engineering, 171 Avelino Tallini, Lajeado, Rio Grande do Sul, Brazil.

+Corresponding author: Simone Stulp, Phone: +55 51 3714-7025, email address: stulp@univates.br

ARTICLE INFO

Article history:
Received: March 19, 2019
Accepted: July 25, 2019
Published: November 20, 2019

Keywords:
1. lactic acid
2. electrodialysis
3. ultrafiltration
4. whey

ABSTRACT: Due to the biotechnological value of whey, this work aims at applying the ultrafiltration (UF) and subsequently the electrodialysis (ED) techniques in pilot scale plant. Whey (5% concentration) was treated twice by the UF technique, with a pressure of 4 bar (flow mode 20 L h^{-1}). The permeate obtained was submitted to the ED process, in which 12 V were applied for 4 h. In order to evaluate the UF, parameters as turbidity, color, TOC and pH were measured. Regarding the ED technique, parameters as pH, conductivity, calcium, sodium and lactic acid concentration were evaluated. The electrodialysis unit was operated on a constant voltage, and tested the range was from 3 to 12 V. After the UF and ED processes, the pH remained unchanged. Thereafter the UF treatment, the initial turbidity was reduced by 99.9%. In terms of parameter reduction after ED, the calcium concentration was decreased in 36.0% soon after UF and ED treatments, and the lactic acid concentration in 80.0%. These results point to the possible combination of UF and ED to treat the whey and signals the potential of further using the resulting solutions as inputs in new applications in the food industry such as lactose.

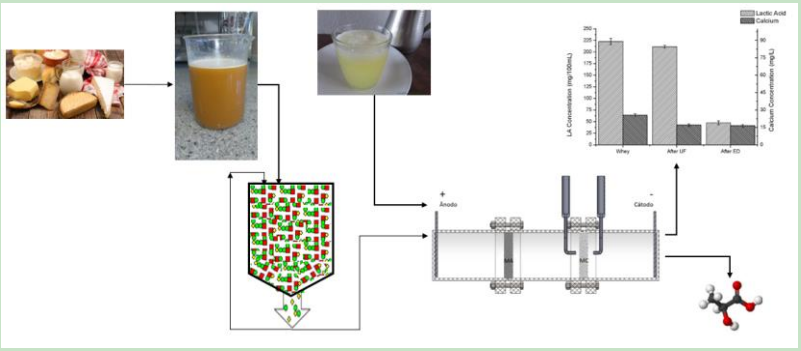

1. Introduction

Whey is one of the by-products of high added value in the dairy industry, by the expressive volume generated as well as by its composition, containing important nutrients. In this process[1], there is no total feedstock conversion in final product, hence, for each kilogram of cheese produced, an average of 10 liters of whey is generated. The milk whey consists, basically, of 94 to 95% water, 3.8 to 4.9% lactose, 0.8 to 1.0% protein and 0.7 to 0.8% of minerals[2]. In terms of Chemical Oxygen Demand (COD), the content of organic compounds is around 60,000 mg L^{-1} [3].

According to some authors[4-6], there are numerous current alternatives for the use of fresh milk whey and its components. Among the alternatives, it can be mentioned, for example, animal feed, production of ricotta, dairy drink, whey powder production, which can be also used in the pharmaceutical industry.

One of the main stages to produce biotechnological products is drying out the whey using a spray dryer equipment. The presence of lactic acid in whey (containing lactate ions) promotes products that are more susceptible to moisture absorption[7], because of the hygroscopic behavior. This phenomenon allows the formation of powdered agglomerates that cannot be tolerated in this process.

The membrane separation processes (MSP) go through clean technology which play an important role in the separation of whey components[8], such as proteins and lactose with subsequent drying.

Such components both contribute to the environment improvement and provide gains to industries. In addition, they are more valued when segregated.

Ultrafiltration (UF) is an alternative and attractive method, since it does not use heat as well as a phase change. This technique is usually applied to retain macromolecules and has been widely used in the dairy industry for the recovery of important components and compounds[9,10]. The UF allows the concentration variance among different compounds, due to the protein retention and selective permeation of lactose, minerals, water and compounds of low molar mass.

Electrodialysis (ED) is an electrochemical technique and shows benefits when compared to traditional processes, since it does not require phase change or addition of chemical reagent, as well as its operational cycle is continuous. It has been widely used in water and wastewater treatment for the removal of ions, for example, ionic species in solution are transported in compartments of a cell through ion-selective, anionic and cationic membranes by the action of an electric field. In addition to this, electrodialysis is an alternative[11,12], method of lactose separation and concentration, when whey solutions are used.

In this context, the aim of this study is to investigate the potential applicability of combining ultrafiltration and ED techniques (in a pilot scale system), in order to remove lactic acid (LA) and other ions from whey, focusing on biotechnological applications.

2. Materials and methods

The research consisted in the recovery of whey (5% concentration) and the purification treatment was carried out twice by the UF technique, in a pilot scale plant (flow mode 20 L h^{-1}), and the permeate obtained was submitted to the ED process in a prototype pilot scale (Fig. 1).

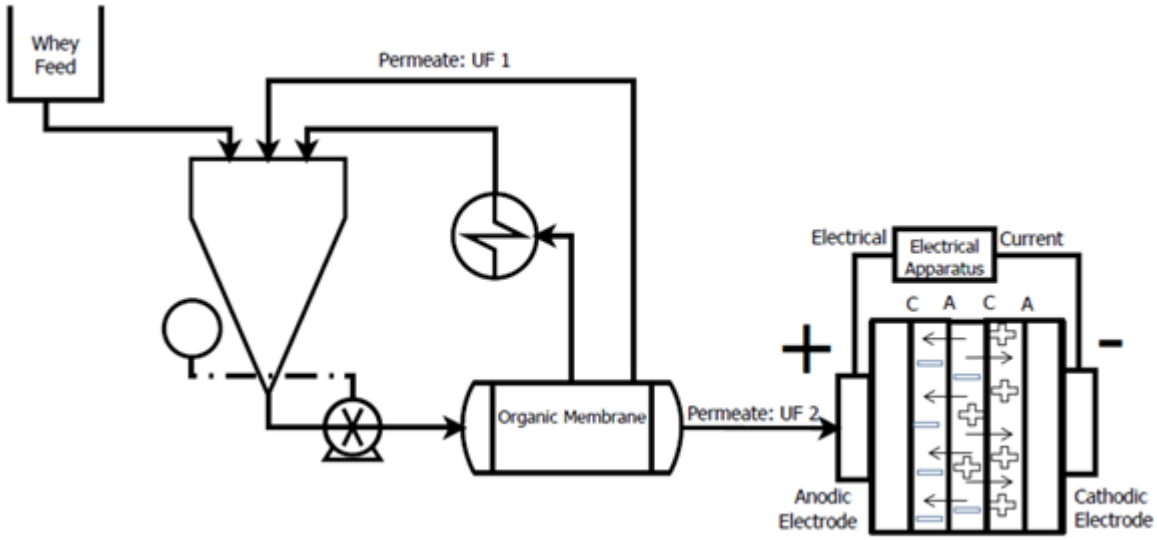

Figure 1. Schematic diagram of ultrafiltration and electrodialysis treatments.

In the ultrafiltration experiments, the volume of permeate was evaluated, and it was collected to determine the flux. In addition, the whey was ultrafiltered under varied conditions, i.e., pH ranging from 5.9 to 7.0 and transmembrane pressure (TMP) ranging between 3.5 and 5.0 bar. After this evaluation, the TMP was maintained at 4 bar and pH 5.9. The UF membrane was AG1812, made of polyethersulfone, manufactured by GE Water. The molar weight cut-off was 200 kDa, and permeation area was 0.37 m^2. The UF experiments were conducted in batch processing. In this process, the concentrate stream return to the begin, like total recirculation mode. The whey was ultrafiltered two times.

After UF treatments, the permeate obtained was submitted to the ED process, in which 12 V were applied for 1 h (for evaluation) and 4 h (total treatment time), in an acrylic cell containing five compartments (total volume of 7 L). In this system, the cathode was a titanium plate and the anode, a $70TiO_2/30RuO_2$ plate (189 cm^2). The

Eclética Química Journal, vol. 44, special issue, 2019, 39-45
ISSN: 1678-4618
DOI: 10.26850/1678-4618eqj.v44.1SI.2019.p39-45

electrodialysis cell was operated on a constant electrochemical potential, and the potential range was 3 to 12 V. The area per ion exchange membrane (AMV and CMV Selemion) was 63.61 cm^2.

2.1 Analysis of limiting current in ED process

Initially, the limiting current in ED process has been determined using a $CaCl_2$ solution for comparison with the results of Na^+ ions, according to the Tanaka[14], in a cation-exchange membrane, to simulate Ca^{2+} ions present in whey. In this evaluation, a constant current source ICEL PS-7000 was used to apply successive increments of electrical current each two-minute intervals, in a cell containing 0.1 mol L^{-1} $CaCl_2$ solution. The cationic membrane potentials were measured (multimeter MINIPA ET-2081) using a multimeter connected to two reference electrodes (Ag/AgCl/KClsat) with Luggin capillary placed at the membrane's interfaces (in a three-compartment acrylic cell). In this experiment, the cathode was a titanium plate and the anode a $70TiO_2/30RuO_2$ plate (8.9 cm^2). At the end of each interval data of applied current, potential of the system and membrane were recorded.

2.2 Sample analysis

The parameters evaluated for the UF treatments were: turbidity (Digimed DM TU), Total Organic Carbon – TOC (Shimadzu TOC-V_{CPH}), Total Nitrogen (Shimadzu TNM-1), Color (Co-Pt), conductivity (856 Metrohm Module) and pH (827 pH Lab Metrohm). For the ED technique, the parameters evaluated were pH and conductivity. A HPLC Shimadzu, LC-20AT, detector DAD: SPD M20A, Autosampler: SIL-20A HT with Supelcogel C-610H; 0.8 mL min^{-1} H_2SO_4 0.05 mol L^{-1}, temperature = 50 °C, λ = 207 nm, retention time = 9.90 min, was used to detect lactate ions[6]. Calcium ions were detected by an Atomic Absorption Spectrometer (Perkin Elmer PinAAcle 900T), λ = 422.67 nm.

3. Results and discussion

3.1 Evaluation of ultrafiltration and ED treatments

To evaluate the efficiency of UF and ED techniques, some initial parameters were analyzed.

3.1.1 Evaluation of ultrafiltration conditions

The results of water and whey flux *vs.* transmembrane pressure are shown in Fig. 2. It is possible to observe that the water flow increased linearly in function of the TMP (r^2 = 0.9229), and for whey solutions the behavior was linear with different slope. The same behavior was found in another study[13].

The transmembrane pressure during Ultrafiltration process was optimal at 4.0 bar. Lower pressure resulted in a decreased flow, in function of lower driving[15]. Also, previous studies showed that higher values of pressure promote an irreversible fouling[16].

Eclética Química Journal, vol. 44, special issue, 2019, 39-45
ISSN: 1678-4618
DOI: 10.26850/1678-4618eqj.v44.1SI.2019.p39-45

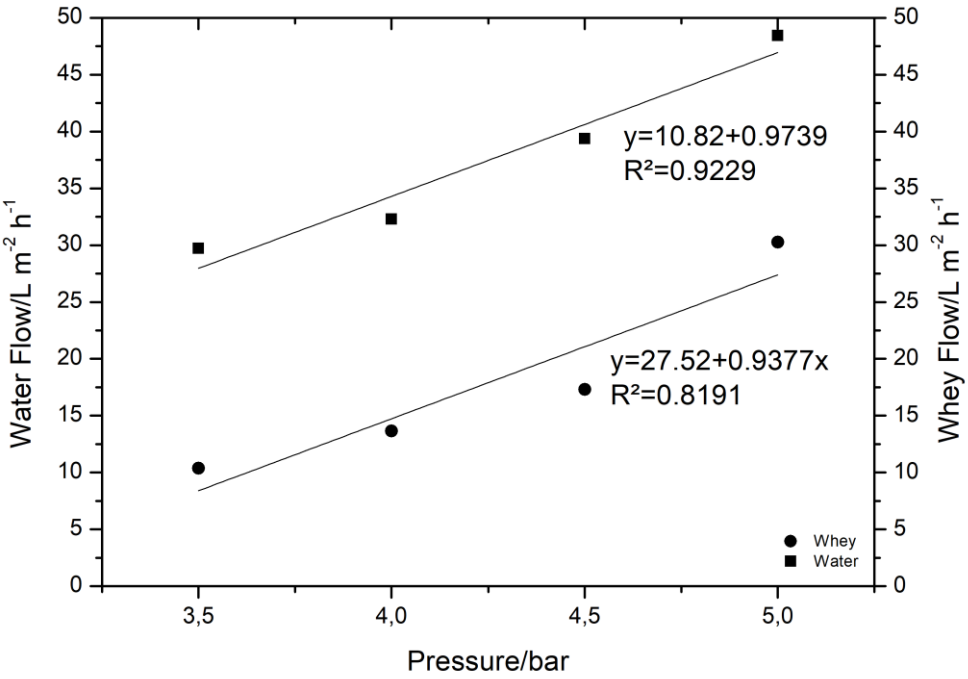

Figure 2. Water and whey flux *vs* transmembrane pressure. Membrane AG1812, T=25 °C, feed flow rate= 20 L h^{-1}. Legend: (■) water, (●) whey.

The evaluation of the ultrafiltration technique was performed by monitoring the turbidity and reduction of color (Co-Pt). In Table 1, results of whey flux (L m^{-2} h^{-1}), reduction of turbidity and color are shown, and in this ultrafiltration system, the best results were obtained using pressure at 4 bar and pH 5.9.

Table 1. Results of experimental conditions and turbidity and color removed after ultrafiltration process

Conditions (pressure and pH)	Whey flux/L m^{-2} h^{-1}	Reduction of turbidity/%	Reduction of color/%
4.0 bar - pH 5.9	15.69	94.81	73.81
4.0 bar – pH 7.0	16.60	92.72	70.54
4;5 bar – pH 5.9	18.83	99.23	67.33

The pH is an important parameter to show the behavior of whey in the ultrafiltration plant. It is a precautionary measure with respect to the range of pH allowed to the membrane. The turbidity and measure of color are quality indicators of solution. The first one is linked to the concentration in colloidal substance in suspension present in the sample and the second one, as well as turbidity also is the result of the light scattering, relatively. The increase of the pressure, hence increase the removal rate of turbidity and decrease the removal rate of color.

These turbidity results are in line with other studies[17,18], when evaluate the ultrafiltration performance for the same endpoint, also find high removal rate. Though, the same dos not occur to the measure of color. This parameter is related to the quality of the treatment, according to another study[13], higher pressure decreases the quality of the permeate.

ISSN: 1678-4618
DOI: 10.26850/1678-4618eqj.v44.1SI.2019.p39-45

3.1.2 Evaluation of electrodialysis conditions

A typical current-potential of the membrane (U_m) curve observed in working ED unit is depicted in Fig. 3, for the electrodialysis of a 0.1 mol L^{-1} $CaCl_2$ solution. For the cationic membranes evaluation, the second region (plateau) in the graphic of Fig. 3 determines a limiting current between 1.79 and 2.02 mA cm^{-2} with cell potential (E_{cell}) around 13 V. After this evaluation, the limiting current was also determined using the work solution (whey), and the results were comparable.

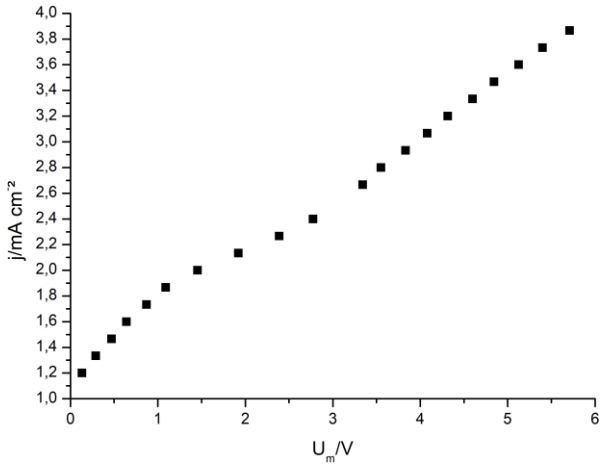

Figure 3. Current-potential of the membrane (U_m) curve observed in working ED unit, for the electrodialysis of a 0.1 mol L^{-1} $CaCl_2$ solution.

In terms of the removal rate of the of Ca^{2+} and Na^+ cations, applying ED treatment for 1 h (for evaluation this treatment), the results are in Table 2, and, in this evaluation, the best results were obtained using a voltage of 12 V. Also, after the ED treatment (operated with a constant 12 V), the initial concentration of lactate ions was reduced in 36.31%. The conductivity of the whey solution (after UF) was around 17.4 mS cm^{-1}.

Table 2. Percentage of ions removed from whey solutions after 60 min of a batch electrodialysis process.

Cell voltage/ V	Removal of Na^+ ions/ %	Removal of Ca^{2+} ions/ %
3	5.91	4.34
6	2.16	9.68
12	13.00	14.63

3.2 Purification and demineralization of whey by UF combined with ED

After the initial evaluation of some parameters in the UF and ED techniques, the purification and demineralization of whey by UF combined with ED were investigated. Fig. 4 shows that the initial flow decays to approximately constant values, from 15.63 L m^{-2} h^{-1} (initially), to 9.5 L m^{-2} h^{-1} (after 80 min), similar results were shown in previous study[19,20].

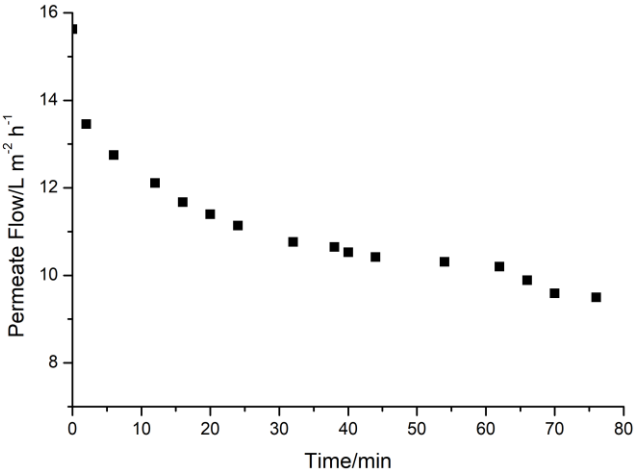

Figure 4. Average flux as a function of time for whey solutions at 4 bar.

The phenomenon of permeation flux reduction must be evaluated to avoid compromising the application of ultrafiltration technique in real systems (scale up). In this study, the whey solution has a pH of 6.2, soluble total organic carbon (TOC) of 8.1 g L^{-1} and total nitrogen of 3.5 g L^{-1}.

The results of concentration in terms of anions (lactate ions) and cations (Ca^{2+}), after ultrafiltration (twice) and electrodialysis treatment (4 h – total time), are shown in Fig. 5. After the electrodialysis process, the conductivity of the treated solution was around 15.69 mS cm^{-1} this result demonstrates the demineralization after ED[6].

Eclética Química Journal, vol. 44, special issue, 2019, 39-45
ISSN: 1678-4618
DOI: 10.26850/1678-4618eqj.v44.1SI.2019.p39-45

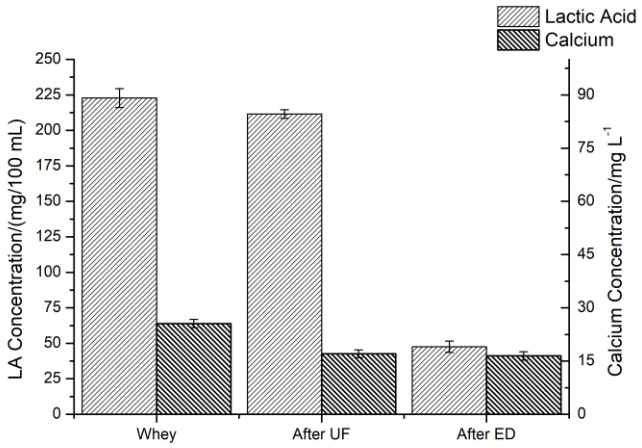

Figure 5. Lactic acid and ion calcium concentration before and after ultrafiltration and ED (4 h).

After the UF and ED processes, the pH remained unchanged, and the initial turbidity was reduced by 99.93%. The calcium concentration was decreased in 36% in the permeate solution, the lactic acid concentration in 80% (after UF + ED), and the TOC was reduced in 56%.

The removal of lactate ions occurs at a slower rate compared to other ions present in whey (when applied ED technique during 1 and 4 h), due to the more complex nature[8,19]. Furthermore, the final calcium concentration (after 4 h) was 41.13 mg L^{-1} and in terms of acid lactic, the final concentration was 43.65 mg/100 mL; and the final acid lactic concentration was 43.65 mg/100 mL; and the decrease of electrical conductivity of the permeate solution is function of time and indicates the efficiency of the ED treatment[21].

These result points to the possible combination of UF and ED to treat the whey and signal the potential of further using the resulting solutions as inputs in new applications in the food industry, such as lactose. In addition, for the whey to be adequately treated by the spray dryer technique, a reduction of the lactic acid concentration is required, being an important step in the milk industry (specially to increase the shelf life).

4. Conclusions

The combination of both methods ultrafiltration (UF) and electrodialysis (ED) is useful to remove the lactic acid and calcium ions from whey, through UF (twice steps) to concentrate and purify lactate, before submitting the permeate in ED treatment (4 h). After the treatments, the initial turbidity was reduced by 99.93%. The calcium concentration was decreased in 36% in the permeate solution, and the lactic acid concentration in 80% (after UF + ED). In UF was observed the membrane fouling phenomenon. This phenomenon occurred because have been colloidal material and macromolecules have been depositing at the membrane surface area promoting a low permeate flux. All these in UF system have been totally depended of pH and transmembrane pressure. In the first minutes of the pilot scale operation, the permeate flow decreased by around 14%. In ED processes, it was also observed this phenomenon. In the same sense of UF, this phenomenon increases the resistance, reducing the efficiency of ED system, and, for this reason, removal rate of the ions from the studied system was modified. These results point to the possible combination of UF and ED to treat the whey and the using of resulting solutions as inputs in new applications, such as lactose.

5. Acknowledgements

This work was developed with institutional infrastructure financed by FAPERGS and CNPq (310253/2016-0, CNPq 465571/2014-0).

6. References

[1] Małgorzata, W., Monika, J., Maria, S. S., Lidia, Z., Fabian, D., Pawel, B., Tomasz, J., Beata, S., ACID whey concentrated by ultrafiltration a tool for modeling bread properties, LWT - Food Science and Technology 61 (1) (2015) 172-176. https://doi.org/10.1016/j.lwt.2014.11.019.

[2] Geoffrey, W. S., Whey and whey proteins-From 'gutter-to-gold', International Dairy Journal 18 (7) (2008) 695-704. https://doi.org/10.1016/j.idairyj.2008.03.008.

[3] Das, M., Raychaudhuri, A., Ghosh, S. K., Supply Chain of Bioethanol Production from Whey: A Review, Procedia Environmental Sciences 35 (2016) 833-846. https://doi.org/10.1016/j.proenv.2016.07.100.

ISSN: 1678-4618
DOI: 10.26850/1678-4618eqj.v44.1SI.2019.p39-45

[4] Salvatore, E., Pes, M., Falchi, G., Pagnozzi, D., Furesi, S., Fiori, M., Roggio, T., Addis, M. F., Pirisi, A., Effect of whey concentration on protein recovery in fresh ovine ricotta cheese, Journal of Dairy Science 97 (8) (2014) 4686-4694. https://doi.org/10.3168/jds.2013-7762.

[5] Díaz-Vergara, L., Pereyra, C. M., Montenegro, M., Pena, G. A., Aminahuel, C. A., Cavaglieri, L. R., Encapsulated whey–native yeast Kluyveromyces marxianus as a feed additive for animal production, Food Additives & Contaminants: Part A 34 (5) (2017) 750-759. https://doi.org/10.1080/19440049.2017.1290830.

[6] Agüero, R., Bringas, E., San Román, M. F., Ortiz, I., Ibáñez, R., Membrane Processes for Whey Proteins Separation and Purification. A Review, Current Organic Chemistry 21 (17) (2017) 1740-1752. https://doi.org/10.2174/1385272820666160927122523.

[7] Saffari, M., Langrish, T., Effect of lactic acid in-process crystallization of lactose/protein powders during spray drying, Journal of Food Engineering 137 (2014) 88-94. https://doi.org/10.1016/j.jfoodeng.2014.04.002.

[8] Chen, G. Q., Eschbach, F. I. I., Weeks, M., Gras, S. L., Kentish, S. E., Removal of Lactic Acid from Acid Whey Using Electrodialysis, Separation and Purification Technology 158 (2016) 230-237. https://doi.org/10.1016/j.seppur.2015.12.016.

[9] Kumar, P., Sharma, N., Ranjan, R., Kumar, S., Bhat, S. F., Jeong, D. K., Perspective of Membrane Technology in Dairy Industry: A Review, Asian-Australasian Journal of Animal Sciences 26 (9) (2013) 1347-1358. https://doi.org/10.5713/ajas.2013.13082.

[10] Iltchenco, S., Preci, D., Bonifacino, C., Fraguas, E. F., Steffens, C., Panizzolo, L. A., Colet, R., Fernandes, I. A., Abirached, C., Valduga, E., Steffens, J., Whey protein concentration by ultrafiltration and study of functional properties, Ciência Rural 48 (5) (2018) https://doi.org/10.1590/0103-8478cr20170807.

[11] Dlask, O., Václavíkova, N., Electrodialysis with ultrafiltration membranes for peptide separation, Chemical Papers 72 (2) (2017) 261-271. https://doi.org/10.1007/s11696-017-0293-6.

[12] Ndiaye, N., Pouliot, Y., Saucier, L., Beaulieu, L., Bazinet, L., Electroseparation of bovine lactoferrin from model and whey solutions, Separation and Purification Technology 74 (1) (2010) 93-99. https://doi.org/10.1016/j.seppur.2010.05.011.

[13] Baldasso, C., Barros, T. C., Tessaro, I. C., Concentration and purification of whey proteins by ultrafiltration, Desalination 278 (1-3) (2011) 381-386. https://doi.org/10.1016/j.desal.2011.05.055.

[14] Tanaka, Y., Current density distribution and limiting current density in ion-exchange membrane electrodialysis, Journal of Membrane Science 173 (2) (2000) 179-190. https://doi.org/10.1016/S0376-7388(00)00368-9.

[15] Macedo, A., Duarte, E., Pinho, M., The role of concentration polarization in ultrafiltration of ovine cheese whey, Journal of Membrane Science 381 (1-2) (2011) 34-40. https://doi.org/10.1016/j.memsci.2011.07.012.

[16] Konrad, G., Kleinschmidt, T., Faber, W., Ultrafiltration flux of acid whey obtained by lactic acid fermentation, International Dairy Journal 22 (1) (2012) 73-77. https://doi.org/10.1016/j.idairyj.2011.08.005.

[17] Brião, V. B., Tavares, C. R. G., Favaretto, D. P. C., Hemkemeier, M., Ultrafiltration of model and Industrial dairy wastewater, CIATEC Journal 7 (1) (2015) 1-12. https://doi.org/10.5335/ciatec.v7i1.3367.

[18] Mendes, P. R. A., Faria, L. F. F., Avaliação do uso de processos de separação por membranas em efluentes de laticínios pré-tratados por coagulação/floculação in Anais do XX Congresso Brasileiro de Engenharia Química, Bucher Chemical Engineering Proceedings 1 (2) (2015) 15084-15091. https://doi.org/10.5151/chemeng-cobeq2014-0630-24668-181190.

[19] Narong, P., James, A. E., Efficiency of ultrafiltration in the separation of whey suspensions using a tubular zirconia membrane, Desalination 219 (1-3) (2008) 348-357. https://doi.org/10.1016/j.desal.2007.04.057.

[20] Pérez, A., Andrés, L. J., Álvarez, A., Coca, J., J., Hill, C. G., Electrodialysis of whey permeates and retentates obtained by ultrafiltration, Journal of Food Process Engineering 17 (2) (1994) 177-190. https://doi.org/10.1111/j.1745-4530.1994.tb00334.x.

[21] Baldasso, C., Lazzari, L. K., Scopel, B. S., Marczak, L. D. F., Tessaro, I. C., Whey fractionation through the membrane separation process, Separation Science and Technology 51 (11) (2016) 1862-1871. https://doi.org/10.1080/01496395.2016.1188115.

ISSN: 1678-4618
DOI: 10.26850/1678-4618eqj.v44.1SI.2019.p39-45

Eclética Química Journal

Original article
iq.unesp.br/ecletica

| Vol. 44 | special issue | 2019 |

Membraneless ethanol,O_2 enzymatic biofuel cell based on laccase and ADH/NAD^+ bioelectrodes

Paula Gonçalves Fenga, Franciane Pinheiro Cardoso, Sofia Nikolaou, Adalgisa Rodrigues de Andrade+
University of São Paulo (USP), Faculty of Philosophy Sciences and Letters at Ribeirão Preto, Department of Chemistry, 3900 Bandeirantes Ave., 14040-901, Ribeirão Preto, SP, Brazil

+Corresponding author: Adalgisa R. de Andrade, phone: +55(16) 33153725, email address: ardandra@ffclrp.usp.br

ARTICLE INFO

Article history:
Received: May 14, 2019
Accepted: November 7, 2019
Published: November 20, 2019

Keywords:
1. alcohol dehydrogenase
2. laccase
3 mediated Ethanol
4. O_2 biofuel cell
5. membraneless Enzymatic Biofuel Cell
6. PAMAM dendrimer

ABSTRACT: This work describes EtOH,O_2 membraneless enzymatic biofuel cells (EtOH,O_2 M_{less}EBFCs) that employ laccase-based biocathodes and ADH/NAD^+ bioanode. Laccase biocathodes were prepared by immobilizing a polypyrrole film containing different redox mediators (ruthenium and osmium complexes). The bioanode for EtOH,O_2 MlessEBFCs was fabricated by immobilizing multiwalled carbon nanotubes, NAD^+-dependent alcohol dehydrogenase enzyme (ADH), poly-methylene green, and poly(amidoamine) (PAMAM) dendrimer onto a carbon cloth platform. Maximum power density and current density were 21.0 ± 0.2 μW cm^{-2} and 0.15 ± 0.07 mA cm^{-2}, respectively, in PBS (pH 6.5). Lifetime tests conducted for EtOH,O_2 M_{less}EBFCs showed promising perspectives for their future application in miniaturized devices.

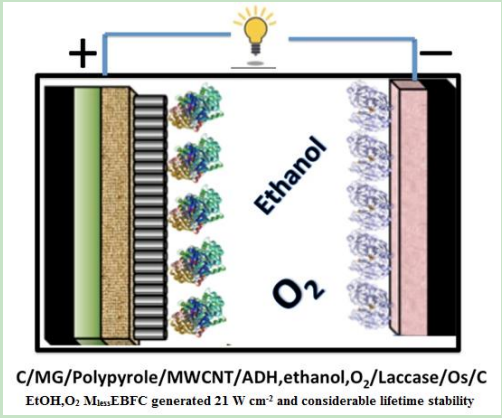

1. Introduction

Biofuel cells (BFCs) employ enzymes or microorganisms as catalysts to convert chemical energy into electric energy. BFCs can operate under milder temperatures (20-40 °C) and physiological pH, so they could be a strategy to replace traditional batteries that need large amount of hazardous metallic catalysts in small devices. Moreover, BFCs could be employed to produce energy from various fuel sources because enzymes can selectively catalyze different fuels[1,2]. Enzymes have high specific selectivity, which could dismiss the need for a membrane[3]. The first report of a membraneless biofuel cell (M_{less}BFC) dates from 1997, when a single compartment cell was used to oxidize organic compounds (sugars or alcohols) while simultaneously reducing molecular oxygen (O_2) at the biocathode[4].

To prepare M_{less}BFCs successfully, enzyme immobilization is a key step to obtain a stable long-lasting device, improving electron transfer kinetics, and increasing power densities (PDs). In this context, researchers have sought to enhance enzymatic system robustness and activity—an enzymatic system must be able to survive pH, temperature, and reaction medium changes. This is not a simple task when one deals with biomolecules, but growing interest in this area has advanced knowledge in the field. A 20-day lifetime has been reported for a membraneless ethanol, oxygen enzymatic biofuel cell (EtOH,O_2 M_{less}EBFC) based on alcohol dehydrogenase (ADH) and bilirubin oxidase (BOD) as bioelectrodes[5]. Over the years, numerous architecture designs for M_{less}EBFCs have been developed in order to achieve higher PD values[6,7]. For instance, Deng and co-workers[8] produced

ISSN: 1678-4618
DOI: 10.26850/1678-4618eqj.v44.1SI.2019.p46-54

energy through oxidation of EtOH present in beverages by employing an EtOH,O_2 M_{less}EBFC. The bioanode MB/AuNPs/PSSG-CHI-ADH was constructed with Meldola's Blue (MB), ADH enzyme, gold nanoparticles (AuNPs), partially sulfonated (3-mercaptopropyl-)trimethoxysilane sol-gel (PSSG), and chitosan (CHI) and an AuNPs/PSSG-CHI–laccase biocathode. The authors described PD of 1.78 mW cm^{-2} at 680 mV when they used wine as fuel, which pointed out that this device deserves attention for alternative energy production.

To increase PD, carbon-based materials, such as multiwalled carbon nanotubes (MWCNTs), have been successfully investigated[9]. With respect to electrochemical performance, MWCNTs are claimed to be more efficient than single-walled carbon nanotubes (SWCNTs). Indeed, MWCNTs have greater surface area and wider potential range, provide many active sites for biomolecule immobilization (which promotes faster electron transfer reactions along the tube axis), and display prominent charge transortation features[10,11].

Immobilization aiming at protein microencapsulation has currently gained researchers' attention. In this immobilization mode, intrinsically conductive polymers and dendrimers are employed as imprisonment arrays so that enzymes are physically entrapped in membrane pores or anchored onto the electrode surface. Intrinsically conductive polymers are compounds that can carry electric current without incorporating conductive charges. Also known as conjugated polymers, their electrical, optical, magnetic, and electronic properties resemble the properties of metals and/or semiconductors. Here, we highlight the use of polypyrrole (polyPYR), which is highly chemically and environmentally stable, biocompatible, and biodegradable. This porous polymer has been widely applied in batteries, sensors, and anti-corrosion protective agents, among others. Several methodologies can be employed to obtain polyPYR layers, and use of this polymer, modified or not, has been often reported[12-14]. Our research group prepared enzymatic biocathode and bioanode for biofuel cells[15,16], and an example of M_{less}EBFCs application can be found elsewhere[17]. PolyPYR and MWCNT matrixes have been employed to prepare glucose,O_2 EBFCs based on glucose oxidase (GOx) and pyrroloquinoline quinone (PQQ) redox mediator absorbed on MWCNTs and polyPYR as a MWCNTs-GOx-PQQ-polyPYR bioanode[17]. PD of 1.1 μW mm^{-2} was achieved at non-compartmentalized BFCs at a cell voltage of 0.167 V in PBS (pH 7.4) for 10 mM glucose (as fuel), and PD of 0.69 μW mm^{-2} was obtained at cell voltage of 0.151 V in human serum containing 5 mmol L^{-1} glucose (37 °C)[17].

PAMAM dendrimer is another promising polymer belonging to the class of branched monodisperse polymers[18,19]. PAMAM has widely uniform structure, low molecular weight, highly functionalized surface and high degree of porosity[19].

We report the construction of a single-chamber EtOH,O_2 biofuel cell to harvest energy from ethanol. Strategies to enhance ET between enzymes and electroactive surfaces include orientation and immobilization of the enzymes and electron mediation. For this laccase-based biocathode metallic redox complexes (Os and Ru) was entrapped in a polyPYR film as redox mediators and the ADH/NAD^+ bioanode employed polymethylene green layer as mediator. We also investigate the activity of the membraneless biofuel for a long period (11 months) in other to show their stability.

2. Experimental

2.1. Chemicals

Enzyme ADH (E.C. 1.1.1.1), from *Saccharomyces cerevisiae* lyophilized powder (331 Units mg^{-1}); enzyme Laccase (E.C. 1.10.3.2.), from *Trametes Versicolor* lyophilized powder (21 Units mg^{-1}); coenzyme nicotinamide adenine dinucleotide hydrate (NAD^+); 2,2´-azinobis(3-ethyl-2,3-dihydrobenzothazole-6-sulfonic acid (ABTS); pyrrole (PYR); and polyamidoamine generation 4 dendrimer (PAMAM) were purchased from Sigma-Aldrich in reactant grade. All reagents and enzymes were used without purification. Enzyme solutions were freshly prepared and rapidly immobilized on the carbon platform.

Multiwalled carbon nanotubes (MWCNTs) were acquired from Cheap Tubes Inc. (diameter of 8.0 nm, length of 10 to 30 μm, and > 95% purity). All solutions were prepared with high-purity water from a Millipore Milli-Q system. Solution pH was measured with a pH electrode coupled to a Qualxtron model 8010 pHmeter.

ISSN: 1678-4618
DOI: 10.26850/1678-4618eqj.v44.1SI.2019.p46-54

2.2. Instrumentation

Electrochemical investigations were conducted on a Potentiostat/Galvanostat AUTOLAB PGSTAT 30 (EcoChemie, Netherlands) at room temperature, (25 ± 1) °C. M_{less}EBFC experiments were carried out in a single-compartment cell (10 mL) by using 200 mmol L^{-1} phosphate buffer solution (PBS) or acetate buffer solution (ABS) at pH 6.5, 1.9 mmol L^{-1} NAD^+, and 100 mmol L^{-1} EtOH as electrolyte.

2.3. Bioelectrode preparation

ADH bioanodes were prepared on carbon cloth platform (HT 1400 w, Elat CDL-Basf), to which MWCNTs and PAMAM were added. Further preparation details can be obtained elsewhere[20].To this end, polymethylene green (poly-MG) was used as immobilized electrocatalyst and was obtained by performing twelve successive voltammetric cycles (−0.3 to 1.3 V vs. Ag/AgCl). After that, a PAMAM anchoring matrix was directly deposited onto the electrode surface, obtained by pippeting 50 µL of 0.025 mol L^{-1} commercial PAMAM solution. Then, 50 µL of MWCNT ink (1 mg of commercial MWCNTs dissolved in EtOH (400 µL) and 100 mmol L^{-1} PBS (600 µL; pH 7.4) and sonicated for at least 4 h) was deposited. After drying, 50 µL of a freshly prepared enzyme solution containing ADH (300 µL; 3.37 mg L^{-1}) + NAD^+ (100 µL; 7.50 mg L^{-1}) + PAMAM (100 µL; 0.025 mol L^{-1}) in PBS (100 µL; 100 mmol L^{-1}; pH 7.4) was cast on the electrode surface. The casting sequence carbon cloth/poly-MG/PAMAM/MWCNTs/ADH was named MWCNTs-ADH configuration.

The osmium $[Os(bpy)_2Cl_2]$ and ruthenium complex $[Ru(bpy)_2Cl_2]$ catalysts for laccase biocathode was synthesized according to the literature[22,23]. $[Os(bpy)_2Cl_2]$ or $[Ru(bpy)_2Cl_2]$ entrapment in polyPYR films (1.5% v/v PYR, 8 mg mL^{-1} $[Os(bpy)_2Cl_2]$ or $[Ru(bpy)_2Cl_2]$ mediator in 100 mmol L^{-1} $NaNO_3$) was accomplished by chronoamperometry at a fixed potential (0.7 V vs. SCE; 10 min). The film containing polyPYR and $[Os(bpy)_2Cl_2]$ or $[Ru(bpy)_2Cl_2]$ mediator was named polyPYR-Os and polyPYR-Ru, respectively.

Laccase biocathodes, which employed $[Os(bpy)_2Cl_2]$ or $[Ru(bpy)_2Cl_2]$ as nanocatalyst and PAMAM dendrimer as enzymatic anchoring matrix, was prepared according to Cardoso and co-workers[15]. To this end, 50 µL of a stock solution, prepared by mixing laccase (300 µL; 3.32 mg mL^{-1}), PAMAM dendrimer (100 µL; 0.025 mol L^{-1}), and acetate buffer solution (ABS; 200 µL; 100 mmol L^{-1}; pH 4), was deposited on the previously modified carbon platform.

Figure 1 displays the representative structures of the bioelectrodes prepared on carbon cloth platforms.

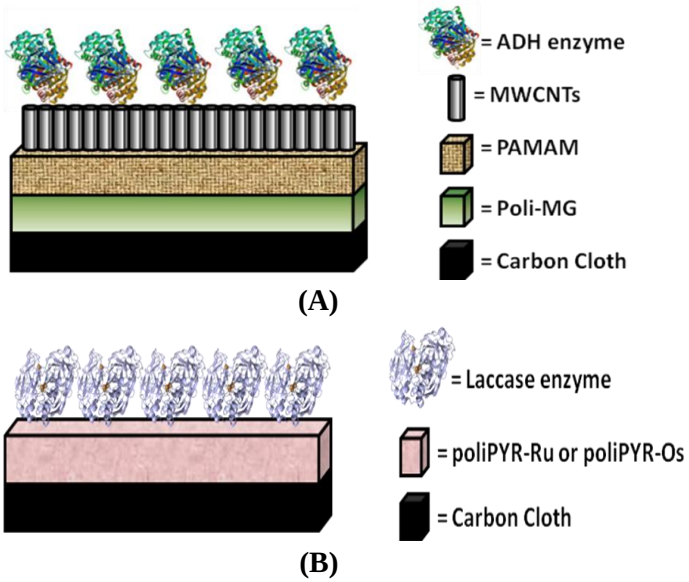

Figure 1. Bioelectrode side schematic representations: A) MWCNTs-ADH Bioanode; B) polyPYR-Os-laccase or polyPYR-Ru-laccase Biocathode.

Bioelectrodes were kept in their appropriate buffer solution (PBS (pH 7.4) for MWCNTs-ADH bioanode or ABS (pH 4.5) for polyPYR-Os-laccase or polyPYR-Os-laccase biocathodes) for at least 24 h before use. After electrochemical experiments, the respective bioelectrodes were kept refrigerated in buffer solution at 4 °C for at least 24 h before a further test was conducted.

pH influence on enzymatic kinetics was determined by assaying laccase and ADH activities at various pH values ranging between 3.5 and 10. To this end, the following 0.1 mol L^{-1} buffer solutions were employed: acetate buffer (NaAc/HAc) for pH 3.5-5, phosphate buffer (NaH_2PO_4/Na_2HPO_4) for pH 6-7, and tris(hydroxymethyl)aminomethane–HCl (Tris+) buffer for pH 8–9. Reaction was initiated by adding substrate to the immobilized protein, depending on the study that was being performed.

ISSN: 1678-4618
DOI: 10.26850/1678-4618eqj.v44.1SI.2019.p46-54

2.4. Biofuel cell tests

Power density measurements were accomplished in an EtOH,O_2 M_{less}EBFC described in the Instrumentation Section. First, the EtOH,O_2 M_{less}EBFC open circuit voltage (OCV) was measured at least 1 h before the cell test. After that, polarization curves at a scan rate of 1 mV s^{-1} were registered in triplicate. PD values for all M_{less}EBFCs were obtained by multiplying cell voltage (E_{cell}) by current density (J_{cell}) (PD = E_{cell} × J_{cell}).

3. Results and discussion

3.1. pH effect on semi- M_{less}EBFC

To obtain maximum M_{less}EBFC performance, it is important to investigate bioelectrode enzymatic behavior as a function of pH because hydrogen ion concentration affects enzymatic activity: enzyme spatial conformation depends on pH values and on the presence of protonated/deprotonated groups in the enzyme catalytic site, which can modify the enzyme tertiary structure. pH also influences intrinsic/extrinsic electron transfer reaction strongly. The individual pH behavior of the immobilized enzymes employed here has previously been investigated in detail[15,20]. The optimum pH range for ADH/NAD^+ bioanode is between 7.0 and 8.0, achieved by employing PBS as buffer[24]. Laccase works best in more acidic medium (pH 4.5), in ABS buffer solution[15]. Therefore, besides operating in different pH ranges, bioanode and biocathode also use distinct buffer solutions.

Direct correlation between enzymatic kinetics and pH is important to obtain maximum bioelectrode performance. Nevertheless, in a M_{less}EBFC both bioelectrodes seldom operate at their optimum pH. To find the best pH for M_{less}EBFC operation, individual pH curves of each enzyme were plotted together (Fig. 2). On the basis of Fig. 2, pH curves intersect at pH 6.5, which was further employed with M_{less}EBFCs. Even though this pH value is close to physiological conditions, other complications may arise and diminish EtOH,O_2 M_{less}EBFC PD and OCV values as compared to separated biofuel cells. Other factors may also be associated with this behavior such as problems with the enzyme-mediator-electrode electron transfer enzyme, which hinders the redox process underlying EtOH oxidation by ADH and O_2 reduction to H_2O by multicopper oxidase enzymes (laccase).

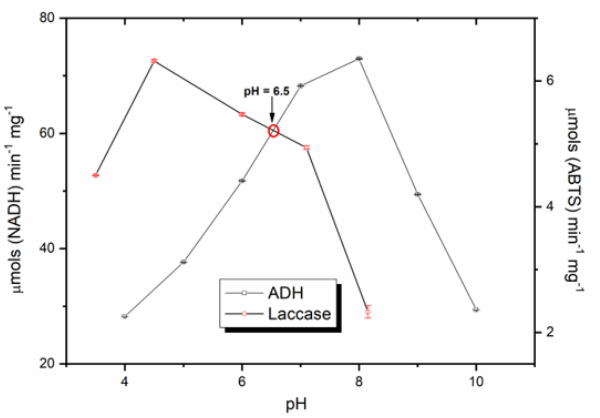

Figure 2. pH influence on the enzymatic activity of bioelectrodes containing immobilized ADH (−■−) in PBS and immobilized laccase (−●−) in ABS.

3.2. EtOH,O_2 membraneless biofuel cell: reaction medium influence (ABS or PBS).

Eliminating proton exchange membrane (PEM) has several advantages. During the reaction process, PEM is subjected to membrane channel obstruction by ions present in the supporting electrolyte, which dries or floods membrane parts, and fuel crossover. To minimize the aforementioned problems, one strategy is to remove the membrane when biocatalyst specificity can be maintained at M_{less}EBFC. However, each bioelectrode must be evaluated for its electron transfer activity and enzymatic selectivity. EtOH,O_2 M_{less}EBFC performance was assessed by analyzing OCV and power density curves obtained from polarization curves (results not shown). To investigate how PBS and ABS buffers influenced M_{less}EBFC activity, EtOH,O_2 M_{less}EBFC performance was measured at pH 6.5 in both buffers (ABS and PBS; buffer concentration = 200 mmol L^{-1}). This “precaution” was necessary because PEM removal resulted in each enzyme facing a medium that was different from its ideal operation condition (ABS (pH 4.5) for laccase and PBS (pH 7.4) for ADH).

Figure 3 shows the results for M_{less}EBFCs containing a MWCNTs-ADH anode and one of the following cathode configurations: polyPYR-Os-laccase or polyPYR-Ru-laccase; either ABS or PBS at pH 6.5 was employed. According to Fig. 3 M_{less}EBFC in PBS buffer operated at higher power density (PD) and current ($J_{cell(max)}$) as compared to M_{less}EBFC in ABS buffer. In PBS buffer (Fig. 3A),

ISSN: 1678-4618
DOI: 10.26850/1678-4618eqj.v44.1SI.2019.p46-54

PD and $J_{cell(max)}$ respectively were 21.0 ± 0.2 μW cm^{-2} and 0.15 ± 0.07 mA cm^{-2} for MWCNTs-ADH, polyPYR-Os-laccase, and 13.5 ± 0.2 μW cm^{-2} and 0.11 ± 0.05 mA cm^{-2} for MWCNTs-ADH,polyPYR-Ru-laccase. When these systems were switched to ABS buffer, both PD and $J_{cell(max)}$ decreased significantly (Fig. 3B). For this reason, PBS was selected as buffer for further EtOH,O_2 M_{less}EBFC investigations.

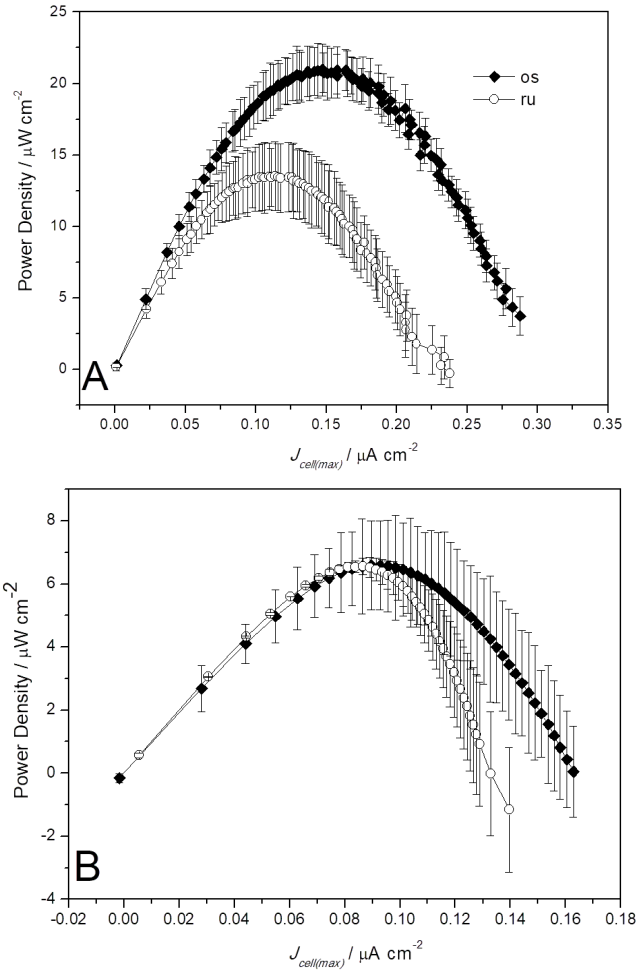

Figure 3. Power density curves for EtOH,O_2 M_{less}EBFCs employing MWCNTs-ADH as bioanode and (−♦−) polyPYR-Os-laccase or polyPYR-Ru-laccase (−○−) as biocathode in (A) PBS and (B) ABS medium (200 mmol L^{-1}; pH 6.5, 1.9 mmol L^{-1} NAD^+, 100 mmol L^{-1} EtOH, n = 3).

3.3. ABTS influence on EtOH,O_2 M_{less}BFCs

ABTS is one of the most common oxygen reduction mediators when laccase is employed in EBFCs. Figure 4 illustrates how ABTS influences EtOH,O_2 M_{less}EBFC performance in PBS medium (pH 6.5) for both anode configurations investigated here: polyPYR-Os-laccase and polyPYR-Ru-laccase.

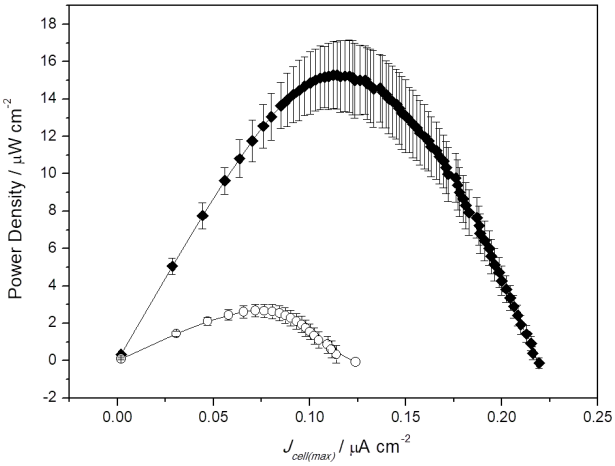

Figure 4. Power density curves for MWCNTs-ADH,polyPYR-Os-laccase (−♦−) and MWCNTs-ADH,polyPYR-Ru-laccase (−○−) in the presence of 1 mmol L^{-1} ABTS (200 mmol L^{-1} PBS (pH 6.5), 1.9 mmol L^{-1} NAD^+, and 100 mmol L^{-1} EtOH; n = 3).

Homogeneous ABTS introduction diminishes Ru-mediated cathode cell PD by over 80% as compared to Os-mediated cathode cell. Indeed, PD decreased from 15.3 ± 0.2 μW cm^{-2} to 2.7 ± 0.3 μW cm^{-2} just by changing the Os complex to the Ru complex. Also, when results obtained in the absence (Fig. 3A) and in the presence (Fig. 4) of ABTS are compared for Os-complex in PBS, PD and $J_{cell(max)}$ was approximately 27.5 and 23.8%, respectively. This decrease could be explained by competition between ABTS and mediators incorporated into the polyPYR matrix and the enzymatic redox sites. The best results were achieved for EtOH,O_2 M_{less}EBFCs based on the MWCNT-ADH,polyPYR-Os-laccase system. These results agreed with literature data[25] claiming that [Os(bpy)$_2$Cl$_2$] can bind to laccase copper hydrophobic T1 active site and establish a strong electrostatic interaction, which entraps the Os-complex in polyPYR, shifts the polyPYR-Os oxidation potential (E_{oxi}), and facilitates electron transfer. Our results showed that polyPYR-Ru-laccase did not interact in the same way as the Os-mediator.

Table 1 summarizes all experimental parameters obtained for EtOH,O_2 M_{less}EBFCs as a function of the different redox mediators entrapped in polyPYR, in the absence or presence of 1 mmol L^{-1} ABTS.

ISSN: 1678-4618
DOI: 10.26850/1678-4618eqj.v44.1SI.2019.p46-54

Table 1. Parameters obtained for different EtOH/O_2 M_{less}EBFCs.

MlessEBFCs	OCV/V	E_{MAX}/V	$J_{cell(max)}$/mA cm^{-2}	PD*/μW cm^{-2}
MWCNTs-ADH,polyPYR-Os-laccase (without ABTS)	0.226 ± 0.008	0.14 ± 0.01	0.15 ± 0.07	21.0 ± 0.2
MWCNTs-ADH,polyPYR-Os-laccase (with ABTS)	0.15 ± 0.06	0.11 ± 0.04	0.11 ± 0.05	15.3 ± 0.2
MWCNTs-ADH,polyPYR-Ru-laccase (without ABTS)	0.17 ± 0.02	0.115 ± 0.006	0.11 ± 0.05	13.5 ± 0.2
MWCNTs-ADH,polyPYR-Ru-laccase (with ABTS)	0.048 ± 0.007	0.037 ± 0.008	0.072 ± 0.001	2.7± 0.3

*Average and standard deviation for combinatorial analysis, in triplicate, for a set of three biocathodes and four bioanodes.

On the basis of the results above (Table 1), the best EtOH,O_2 M_{less}EBFCs was MWCNTs-ADH,polyPYR-Os-laccase in 200 mmol L^{-1} PBS (pH 6.5) in the absence of ABTS. Figure 5 illustrates the selected operation system.

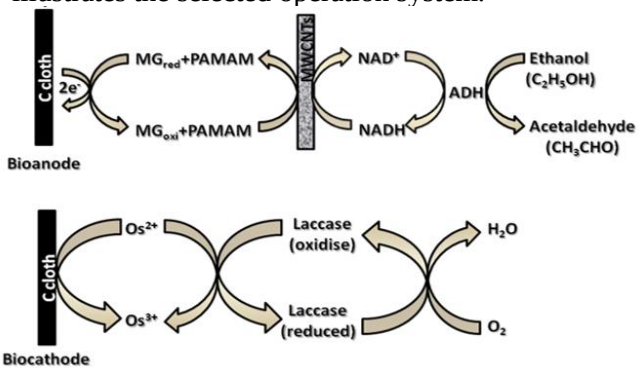

Figure 5. Schematic diagram of mediated electron transfer in EtOH,O_2 M_{less}EBFCs based on MWCNTs-ADH,polyPYR-Os-laccase.

We have investigated and reported half-cell data for these electrodes configuration before[15,21]. For the biocathode half-cell[15] a gas diffusion membrane (ELAT) consisting of 40% metal in C (Pt0.66Ru0.34, E-TEK commercial mixture) hot pressed in a Nafion NRE-212 membrane was employed as the anode. This configuration furnished at least five times higher power densities values than the value reported for the membraneless fuel cell. For the half-bioanode[21] Pt was used as cathode, also separated by a Nafion membrane. This configuration furnished power density values as high as 0.25 mW cm^{-2}. Table 1 shows that the results for EtOH,O_2 M_{less}EBFCs are much lower than the separated compartment cell indicating that besides pH effect must be a mutual influence of the fuel and O_2 in the performance of the enzymatic systems. Nevertheless, despite differences with respect to enzyme immobilization method, the values measured herein are in the same order of magnitude (μW cm^{-2}) with some data reported in the literature data[5,8,27,28]. Considering the high efficiency in ethanol/acetaldehyde conversion and concomitant O_2 reduction to H_2O demonstrated by enzymatic systems future application of biofuel cells in miniaturized systems must be solved preparing microfluidic devices that operate with streams of liquid electrolytes[29]. In this configuration it is possible to operate with different electrolytes for anodic and cathodic compartments without any problem. This is our future goal to increase the power density.

Table 2 lists the MWCNTs-ADH,polyPYR-Os-laccase cell storage lifetime under optimum conditions (200 mmol L^{-1} PBS (pH 6.5), 1.9 mmol L^{-1} NAD^+, and 100 mmol L^{-1} EtOH).

Table 2. EtOH,O_2 M_{less}EBFCs storage lifetime for polyPYR-Os-Laccase and MWCNTs-ADH bioelectrodes.

M_{less}EBFC	OCV/V	$J_{cell(max)}$/mA cm^{-2}	PD*/μW cm^{-2}
Fresly produced	0.226 ± 0.008	0.15 ± 0.07	21.0 ± 0.2
After 5 months	0.198 ± 0.003	0.09 ± 0.02	13 ± 4
After 11 months	0.140 ± 0.02	0.08 ± 0.02	8 ± 2

*Average and standard deviation analysis, in triplicate, for a set of three biocathodes and four bioanodes.

ISSN: 1678-4618
DOI: 10.26850/1678-4618eqj.v44.1SI.2019.p46-54

After five months, PD and $J_{cell(max)}$ decreased by approximately 38% (13 ± 4) μW cm^{-2} and 0.09 ± 0.02 mA cm^{-2}, respectively) as compared to freshly prepared electrodes. These values dropped slowly and reached 62% and 48% (8 ± 2 μW cm^{-2} and 0.09 ± 0.02 mA cm^{-2}, respectively) of the initial values. These results attested that immobilization of the enzymes employed here provided a relatively stable medium for long-term storage tests. This result may be important to apply these devices in new types of nanofluid cells to enhance the power harvest from the ethanol molecule[30].

4. Conclusions

Bioelectrodes containing the enzymes ADH and laccase and different redox mediators (Os or Ru) entrapped in polyPYR films or PAMAM dendrimer were tested. MWCNTs-ADH,polyPYR-Os-laccase employing PBS (pH 6.5) in the absence of ABTS performed the best. PD and $J_{cell(max)}$ remained around 21.0 ± 0.2 μW cm^{-2} and 0.15 ± 0.07 mA cm^{-2} for freshly prepared electrodes. Electrodes retain 38% of their activity after storage for five months storage in a refrigerator. The prepared EtOH,O_2 M_{less}EBFC generated power densities values comparable with literature data as well as considerable lifetime stability. Therefore, the results presented here for EtOH,O_2 M_{less}EBFCs are promising and may be employed in microfluidic devises to enhance the activity of the system.

5. Acknowledgments

Financial support from CAPES (PNPD 2779/2010 and 001 grants), FAPESP (Grant # - 2014/04813-9), and CNPq (400712/2014-8) are gratefully acknowledged.

6. References

[1] Rasmussen, M., Abdellaoui, S., Minteer, S. D., Enzymatic biofuel cells: 30 years of critical advancements, Biosensors and Bioelectronics 76 (15) (2016) 91-102. https://doi.org/10.1016/j.bios.2015.06.029.

[2] Aquino Neto, S., Andrade, A. R., New energy sources: The enzymatic biofuel cell, Journal of the Brazilian Chemical Society 24 (12) (2013) 1891-1912. https://doi.org/10.5935/0103-5053.20130261.

[3] Minteer, S. D., Liaw, B. Y., Cooney, M. J., Enzyme-based biofuel cells, Current Opinion in Biotechnology 18 (3) (2007) 228-234. https://doi.org/10.1016/j.copbio.2007.03.007.

[4] Ghindilis, A. L., Atanasov, P., Wilkins, E., Enzyme catalyzed direct electron transfer: Fundamentals and analytical applications, Electroanalysis 9 (9) (1997) 661-674. https://doi.org/10.1002/elan.1140090902.

[5] Topcagic, S., Minteer, S. D., Development of a membraneless ethanol/oxygen biofuel cell, Electrochimica Acta 51 (11) (2006) 2168-2172. https://doi.org/10.1016/j.electacta.2005.03.090.

[6] Falk, M., Blum, Z., Shleev, S., Direct electron transfer based enzymatic fuel cells, Electrochimica Acta 82 (2012) 191-202. https://doi.org/10.1016/j.electacta.2011.12.133.

[7] Shao, M., Zafar, M. N., Falk, M., Ludwig, R., Sygmund, C., Peterbauer, C. K., Guschin, D. A., Conghaile, P. O., Leech, D., Toscano, M. D., Shleev, S., Schuhmann, W., Gordon, L., Optimization of a membraneless glucose/oxygen enzymatic fuel cell based on a bioanode with high coulombic efficiency and current density, ChemPhysChem 14 (10) (2013) 2260-2269. https://doi.org/10.1002/cphc.201300046.

[8] Deng, L., Shang, L., Wen, D., Zhai, J., Dong, S., A membraneless biofuel cell powered by ethanol and alcoholic beverage, Biosensors and Bioelectronics 26 (1) (2010) 70-73. https://doi.org/10.1016/j.bios.2010.05.007.

[9] Poulpiquet, A., Ciaccafava, A., Lojou, E., New trends in enzyme immobilization at nanostructured interfaces for efficient electrocatalysis in biofuel cells, Electrochimica Acta 126 (2014) 104-114. https://doi.org/10.1016/j.electacta.2013.07.133.

[10] Cai, H., Cao, X., Jiang, Y., He, P., Fang, Y., Carbon nanotube-enhanced electrochemical DNA biosensor for DNA hybridization detection, Analytical and Bioanalytical Chemistry 375 (2003) 287-293. https://doi.org/10.1007/s00216-002-1652-9.

[11] Li, N., Duan, J., Chen, G., Determination of trace procaine hydrochloride by differential pulse adsorptive stripping voltammetry with a Nafion modified glassy carbon electrode, Analytical Sciences 19 (12) (2003) 1587-1592. https://doi.org/10.2116/analsci.19.1587.

[12] Baur, J., Holzinger, M., Gondran, C., Cosnier, S., Immobilization of biotinylated biomolecules onto electropolymerized poly(pyrrole-nitrilotriacetic acid)–Cu^{2+} film, Electrochemistry Communications 12 (10) (2010) 1287-1290. https://doi.org/10.1016/j.elecom.2010.07.001.

ISSN: 1678-4618
DOI: 10.26850/1678-4618eqj.v44.1SI.2019.p46-54

[13] Papper, V., Gorgy, K., Elouarzaki, K., Sukharaharja, A., Cosnier, S., Marks, R. S., Biofunctionalization of Multiwalled Carbon Nanotubes by Irradiation of Electropolymerized Poly(pyrrole–diazirine) Films, Chemistry A European Journal 19 (29) (2013) 9639-9643. https://doi.org/10.1002/chem.201300873.

[14] Endrődi, B., Kormányos, C. J., Janáky, C., Berkesi, O., Visy, C., Fixation of laccase enzyme into polypyrrole, assisted by chemical interaction with modified magnetite nanoparticles: A facile route to synthesize stable electroactive bionanocomposite catalysts, Electrochimica Acta 122 (10) (2014). https://doi.org/10.1016/j.electacta.2013.08.175.

[15] Cardoso, F. P., Aquino Neto, S., Crepaldi L. B., Nikolaou, S., Barros, V. P., Andrade, A. R., Biocathodes for Enzymatic Biofuel Cells Using Laccase and Different Redox Mediators Entrapped in Polypyrrole Matrix. Journal of the Electrochemical Society 161 (2014) F445–F450. https://doi.org/10.1149/2.041404jes.

[16] Crepaldi, L. B., Aquino Neto, S., Cardoso, F. P., Ciancaglini, P., Andrade, A. R., Ferrocene entrapped in polypyrrole film and PAMAM dendrimers as matrix for mediated glucose/O_2 biofuel cell, Electrochimica Acta 136 (2014) 52-58. https://doi.org/10.1016/j.electacta.2014.05.049.

[17] Ammam, M., Fransaer, J., Micro-biofuel cell powered by glucose/O_2 based on electro-deposition of enzyme, conducting polymer and redox mediators: Preparation, characterization and performance in human serum, Biosensors and Bioelectronics 25 (6) (2010) 1474-1480. https://doi.org/10.1016/j.bios.2009.11.001.

[18] Forti, J. C., Aquino Neto, S., Zucolotto, V., Ciancaglini, P., Andrade, A. R., Development of novel bioanodes for ethanol biofuel cell using PAMAM dendrimers as matrix for enzyme immobilization, Biosensors and Bioelectronics 26 (5) (2011) 2675-2679. https://doi.org/10.1016/j.bios.2010.05.011.

[19] Perinotto, A. C., Caseli, L., Hayasaka, C. O., Riul Júnior, A., Oliveira Júnior, O. N., Zucolotto, V., Dendrimer-assisted immobilization of alcohol dehydrogenase in nanostructured films for biosensing: Ethanol detection using electrical capacitance measurements, Thin Solid Film 516 (24) (2008) 9002-9005. https://doi.org/10.1016/j.tsf.2007.11.087.

[20] Aquino Neto, S., Forti, J. C., Zucolotto, V., Ciancaglini, P., Andrade, A. R. Development of nanostructured bioanodes containing dendrimers and dehydrogenases enzymes for application in ethanol biofuel cells, Biosensors and Bioelectronics 26 (6) 2922-2926 (2011). https://doi.org/10.1016/j.bios.2010.11.038.

[21] Fenga, P. G., Cardoso, F. P., Aquino Neto, S., Andrade, A. R., Multiwalled carbon nanotubes to improve ethanol/air biofuel cells. Electrochimica Acta 106 (2013) 109-113. https://doi.org/10.1016/j.electacta.2013.05.046.

[22] Johnson, E. C., Sullivan, B. P., Salmon, D. J., Adeyemi, S. A., Meyer, T. J., Synthesis and properties of the chloro-bridged dimer [(bpy)2RuCl]22+ and its transient 3+ mixed-valence ion, Inorganic Chemistry 17 (8) (1978) 2211-2215. https://doi.org/10.1021/ic50186a038.

[23] Kober, E. M., Caspar, J. V, Sullivan, B. P., Meyer, T. J., Synthetic routes to new polypyridyl complexes of osmium(II). Inorganic Chemistry 27 (25) (1988) 4587-4598. https://doi.org/10.1021/ic00298a017.

[24] Aquino Neto, S., Forti, J. C., Zucolotto, V., Ciancaglini, P., Andrade, A. R., The kinetic behavior of dehydrogenase enzymes in solution and immobilized onto nanostructured carbon platforms, Process Biochemistry 46 (12) (2011) 2347-2352. https://doi.org/10.1016/j.procbio.2011.09.019.

[25] Meredith, M. T., Minteer, S. D., Biofuel Cells: Enhanced Enzymatic Bioelectrocatalysis, Annual Review of Analytical Chemistry 5 (2012) 157-179. https://doi.org/10.1146/annurev-anchem-062011-143049.

[26] Cardoso, F. P., Aquino Neto, S., Ciancaglini, P., Andrade, A. R., The use of PAMAM dendrimers as a platform for laccase immobilization: Kinetic characterization of the enzyme, Applied Biochemistry and Biotechnology 167 (7) (2012) 1854-1864. https://doi.org/10.1007/s12010-012-9740-6.

[27] Ramanavicius, A., Kausaite, A., Ramanaviciene, A., Enzymatic Fuel Cells: From Fundamentals to Applications, Biosensors and Bioelectronics 20 (10) (2005) 1962-1967. https://doi.org/10.1016/j.bios.2004.08.032.

[28] Das, M., Barbora, L., Das, P., Goswami, P., Biofuel cell for generating power from methanol substrate using alcohol oxidase bioanode and air-breathed laccase biocathode, Biosensors and Bioelectronics 59 (2014) 184-191. https://doi.org/10.1016/j.bios.2014.03.016.

[29] Hashemi, S. M. H., Neuenschwander, M., Hadikhani, P., Modestino, M. A., Psaltis, D., Membrane-less micro fuel cell based on two-phase flow, Journal of Power Sources 348 (2018) 212-218. https://doi.org/10.1016/j.jpowsour.2017.02.079.

[30] Escalona-Villapando, R. A., Martínez-Maciel, A. C., Espinosa-Ángeles, J. C., Ortiz-Ortega, E., Arjona, N.,

ISSN: 1678-4618
DOI: 10.26850/1678-4618eqj.v44.1SI.2019.p46-54

Arriaga, L. G., Ledesma-Garcia, J., Evaluation of hyrid and enzymatic nanofluidic fuel cells using 3D carbon structures, International Journal of Hydrogen Energy 43 (26) (2018) 11847-11852. https://doi.org/10.1016/j.ijhydene.2018.04.016.

ISSN: 1678-4618
DOI: 10.26850/1678-4618eqj.v44.1SI.2019.p46-54